Mineralium Deposita (2019) 54:959–982
https://doi.org/10.1007/s00126-018-0849-6

ARTICLE

The geometallurgical assessment of by-products—geochemical proxies for the complex mineralogical deportment of indium at Neves-Corvo, Portugal

Max Frenzel[1,2] · Kai Bachmann[1] · João R. S. Carvalho[3] · Jorge M. R. S. Relvas[4] · Nelson Pacheco[5] · Jens Gutzmer[1]

Received: 29 September 2018 / Accepted: 10 October 2018 / Published online: 23 November 2018

Abstract

Many by-product metals are classified as critical. However, they are only of marginal interest to many mining companies and are rarely part of detailed resource statements or geometallurgical assessments. As a result, there is a general lack of reliable quantitative data on the mineralogy and spatial distribution of these metals in ore deposits—hampering assessments of future availability. We propose here an innovative approach to integrate by-product metals into geometallurgical assessments. As an example, we use the distribution and deportment of indium at Neves-Corvo, a major European base-metal mine (Cu + Zn), and one of the largest and richest volcanic-hosted massive sulfide (VHMS) deposits in the world. Based on a combination of bulk-ore geochemistry and mineralogical and microanalytical data, this study is the first to develop a quantitative model of indium deportment in massive sulfide ores, demonstrating how regularities in indium partitioning between different minerals can be used to predict its mineralogical deportment in individual drill-core samples. Bulk-ore assays of As, Cu, Fe, Pb, S, Sb, Sn, Zn, and In are found to be sufficient for reasonably accurate predictions. The movement of indium through the ore processing plants is fully explained by its mineralogical deportment, allowing for specific mine and process planning. The novel methodologies implemented in this contribution for (1) the assessment of analytical uncertainties, (2) the prediction of complex mineralogical deportments from bulk geochemical data, and (3) the modeling of by-product recoveries from individual mining blocks, are of general applicability to the geometallurgical assessment of many other by-product metals in polymetallic sulfide ores, including Ga, Ge, Mo, Re, Se, Te, as well as the noble metals.

Keywords Geometallurgy · By-products · Trace elements · Automated mineralogy · Mineral balances · VMS deposits · VHMS deposits

Editorial handling: B. Lehmann

Electronic supplementary material The online version of this article (https://doi.org/10.1007/s00126-018-0849-6) contains supplementary material, which is available to authorized users.

✉ Max Frenzel
m.frenzel@hzdr.de

[1] Helmholtz-Institute Freiberg for Resource Technology, Chemnitzer Str. 40, 09599 Freiberg, Germany

[2] Institute of Mineralogy, Technische Universität Bergakademie Freiberg, Brennhausgasse 14, 09599 Freiberg, Germany

[3] Sustainable Innovation Centre, ISQ, Oeiras Taguspark, 2740-120 Porto Salvo, Portugal

[4] Instituto Dom Luiz, Faculdade de Ciências, Universidade de Lisboa, 1749-016 Lisbon, Portugal

[5] SOMINCOR, Sociedade Mineira de Neves-Corvo, S.A., Mina de Neves-Corvo, Santa Bárbara de Padrões, Apartado 12, 7780-409 Castro Verde, Portugal

Introduction

Despite their potential to generate significant additional revenue at some mines, as well as their importance for the global economy (Wellmer et al. 1990; Nassar et al. 2015; EU Commission 2017), many by-product metals are only of marginal interest to most mining companies. Detailed quantitative information on their spatial distribution and geometallurgical behavior in relevant ore deposits is therefore lacking (e.g., Werner et al. 2017).

Indium is a prime example of such a metal. Not only is it considered a critical raw material by most authors (e.g., Graedel et al. 2015; NSTC 2016), but unlike other by-products, such as gallium and germanium, it is also approaching its theoretical production limit (Frenzel et al. 2017). This means that there is a high probability for persistent future shortages. Despite these issues, only a limited amount of information is

available on its occurrence in base-metal sulfide ores, the major primary source material (Schwarz-Schampera and Herzig 2002; Frenzel et al. 2017). Specifically, there are no detailed quantitative studies of its mineralogical deportment in such ores, how this impacts recovery and extraction, and whether it follows predictable regularities. This information is necessary to evaluate potential options to increase recoveries and meet rising demand (Werner et al. 2017).

In general, this kind of understanding is necessary to efficiently incorporate by-product metals into existing geometallurgical models (e.g., Boisvert et al. 2013). Efficiency is key since mining companies will not generally be able to invest a sizeable proportion of their research and development budgets into the acquisition of by-product-specific data.

The major aim of this study was to develop a suitable methodology for this purpose, using the case of indium in the Neves-Corvo deposit, Portugal, as an example. We achieve our aim by combining data from bulk-ore geochemistry, scanning-electron-microscope-(SEM)-based image analysis, and electron probe microanalysis (EPMA) for a comprehensive set of ore and processing samples. By starting the investigation with actual ore samples, and not the blended feed materials entering the processing plant, we are able to develop predictive models for indium deportment in individual mining blocks that allow for the planning of the extraction, recovery, and commercialization of the mine's indium content.

While equivalent results for mineralogical deportments have been achieved for gold (e.g., Chryssoulis and Cabri 1990; Gregory et al. 2013) and the platinum group elements (PGEs, e.g., Cabri et al. 2002; Barnes et al. 2008; Osbahr et al. 2013), this is the first such study of indium. It is also, to the best knowledge of the authors, the first study to include a detailed assessment of analytical uncertainties and to develop a model allowing for the direct prediction of a complex mineralogical deportment from bulk-ore geochemistry. The principles applied in this study easily transfer not only to other by-product commodities (e.g., Ag, Ga, and Ge) but also main products (Au and the PGEs) and penalty elements (e.g., As, Cd, Sb, and Tl).

We chose the Neves-Corvo deposit for this work, because (1) it is a representative of the most important class of indium-hosting base-metal deposits (volcanic-hosted massive sulfide (VHMS) deposits; Frenzel et al. 2017) and (2) it stands out among this deposit class because of its exceptional metal endowment.

With current reserves and resources of 209 Mt at 1.26% Cu, 3.82% Zn, 0.86% Pb, and 51 g/t Ag (Lundin 2017), the total metal content of Neves-Corvo is by far the largest in the Iberian Pyrite Belt (IPB), and one of the largest for any VHMS deposit in the world (Mosier et al. 2009). Based on this exceptional metal endowment, Neves-Corvo is currently one of the most important producers of copper and zinc concentrates in the European Union (Gurmendi 2013). Furthermore, it is well known for its high indium content (e.g., Schwarz-Schampera and Herzig 2002; Relvas et al. 2006a). With current production at 3.5 Mt/a of ore (Lundin 2017) at ~ 40 ppm indium (this study; cf. Carvalho et al. 2018) for a total indium content of ~ 140 t/a, it is probably the largest potential source of primary indium in Europe. It is not clear, however, what proportion of this is extracted at smelters. For comparison, global primary indium production in 2016 was 655 t (Tolcin 2017), probably from a range of different deposit types (Frenzel et al. 2017).

Background

It has long been recognized that mineralogical deportment is a key factor in the recoverability of minor and trace metals from their ores (e.g., Chryssoulis and Cabri 1990), in addition to textural and grinding properties. This is because it controls the proportions reporting to concentrate and waste streams. Most of any metal associated with gangue minerals, e.g., pyrite in the case of VHMS ores, will be lost to tailings.

General principles

The mineralogical deportment of an element k present at a bulk concentration (C_k) in an ore sample consisting of N different minerals, $\{i\}$, is described by the set of percentages:

$$\left\{\frac{c_i \cdot x_i}{C_k} \cdot 100\%\right\}_{i=1,\ \ldots,\ N} \quad (1)$$

where x_i is the modal abundance of mineral i in the sample, and c_i is the concentration of element k in mineral i (cf. Chryssoulis and Cabri 1990; Goodall 2008; Minz et al. 2015; Kern et al. 2018). Because C_k is equal to $C_k = \sum_{i=1}^{N} c_i \cdot x_i$, it is in principle sufficient to determine the values of the c_i and x_i to assess the mineralogical deportment. However, it is also often useful to include an independent assessment of C_k as a check on the completeness of the deportment estimate (Chryssoulis and Cabri 1990).

Previous work on indium mineralogy in base-metal sulfide ores

There are several earlier studies on the mineralogy of indium in samples from Neves-Corvo (Benzaazoua et al. 2002, 2003; Gaspar 2002; Schwarz-Schampera and Herzig 2002; Serranti et al. 2002; Carvalho et al. 2013, 2015, 2018), as well as other VHMS deposits (Burnham 1959; Cabri et al. 1985; Huston et al. 1995; Yi et al. 1995; Schwarz-Schampera and Herzig 2002; Cook et al. 2009, 2011a; Ye et al. 2011; Lockington

et al. 2014; George et al. 2016). All these studies focused exclusively on mineral chemistry ($\{c_i\}$). Thus, their results are of limited use for mineralogical deportment, since mineral abundances ($\{x_i\}$) and bulk indium concentrations (C_k), the other key components in deportment studies, were not assessed. Studies of indium mineralogy in ores from other types of sulfide base-metal deposits generally suffer from the same problem (e.g. Boorman and Abbott 1967; Ohta 1989; Seifert and Sandmann 2006; Sinclair et al. 2006; Cook et al. 2011b; Murakami and Ishihara 2013).

In addition to studies of ore samples, a limited number of studies has been conducted on the processing behavior of indium (Chen and Petruk 1980; Petruk and Schnarr 1981; Benzaazoua et al. 2002). These studies are based on C_k and $\{x_i\}$ in processing materials but do not include detailed information on $\{c_i\}$. As such, they are again limited in terms of the conclusions that can be drawn from them.

Actual indium deportments are only estimated in one recent study (Bachmann et al. 2017). However, the methodological focus of this study means that results are restricted to a small number of ore samples ($n = 5$). Processing samples are not included, and results are not discussed in the context of ore beneficiation.

To summarize, current knowledge on the mineralogical deportment of indium in base-metal sulfide ores is extremely limited. Although a detailed discussion is beyond the scope of this article, we note that similar limitations exist for most other common by-products of sulfide base-metal ores, including Ag, Ga, Ge, Mo, Re, Se, and Te.

The Neves-Corvo deposit

Neves-Corvo is located in the Portuguese part of the Iberian Pyrite Belt (IPB) (Tornos 2006), about 220 km southeast of Lisbon. It consists of seven known sulfide ore bodies (Corvo, Graça, Lombador, Monte Branco, Neves, Semblana, and Zambujal; cf. Fig. 1), hosted within the Volcanic-Sedimentary Complex (VSC), a complex stratigraphic unit containing black shales, felsic volcanic rocks, and hydrothermal exhalite horizons (jasper, carbonate) (Fig. 1). The VSC is underlain by the Phyllite-Quartzite Group (PQ), and overlain by the Baixo-Alentejo Flysch Group (BAF). The sulfide mineralization generally occurs on top of the Neves Formation (black shales), but locally contacts the PQ in the Lombador ore body.

Detailed palynostratigraphic and volcanological studies (Oliveira et al. 2004; Rosa et al. 2008), in conjunction with extensive surface and underground mapping (e.g., Carvalho and Ferreira 1994; Pacheco et al. 1998), have revealed a complex lithostratigraphic sequence within all three major units (the VSC, PQ, and BAF), extending from the Upper Famennian to the Upper Visean. According to these studies, the massive sulfide mineralization is of Upper Famennian age (~ 359–360 Ma) (Oliveira et al. 2004).

Starting in the Upper Visean, the entire sequence was subjected to SE-verging folding and thrusting as part of the Variscan orogeny (Oliveira et al. 2004). This resulted in the complex tectonic stacking, and large-scale long-wavelength folding, of different stratigraphic units observed today (Fig. 1), and has also had a significant effect on the spatial distribution of metals within the deposit (cf. Carvalho et al. 2018). Metamorphic grades no higher than lower greenschist facies were attained during synorogenic deformation (Munhá 1990).

Several ore types are distinguished by the mine geologists based on chemical and mineralogical composition, and texture (cf. Gaspar and Pinto 1991; Gaspar 2002; Relvas et al. 2006a; Carvalho et al. 2018). An overview is provided in Table 1. Figure 2 shows mineral liberation analyzer (MLA)-generated mineral maps of some of the samples studied in this work to illustrate the textural and mineralogical variability these ore types represent.

In general, ores are divided into tin-rich (suffix -T), copper-rich (suffix -C), zinc-rich (suffix -Z), lead-rich (suffix -P), and barren pyrite (suffix -E) types. Ores with more than 50 vol.% of sulfides are classed as massive sulfide ores (prefix M-), while those with less than 50 vol.% sulfides are classed as stockwork ores (prefix F-). The rubané ores (prefix R-) of some previous authors (Gaspar 2002; Relvas et al. 2006a,b) have been subsumed into the stockwork type (cf. Carvalho et al. 2018) and are therefore not listed separately in Table 1. It should be noted that the exact definitions of the chemical boundaries between ore types (tin-rich, copper-rich, etc.) have changed over the years, due to changes in cut-off grades and the structure of the mineral processing plants (Gaspar 2002; Owen and Chilcott 2007; Owen and Meyer 2013; Newall et al. 2017).

At present, the most important ore types for the mine, both by volume and overall metal content, are the copper- and zinc-rich massive sulfide ores (MC, MCZ, MZ, and MZP), as well as the copper-rich stockwork ores (FC) (Newall et al. 2017). Lead-rich massive sulfide ores (MP) are presently not of economic interest, due to their low abundance, and a lack of suitable processing capabilities (Newall et al. 2017). Similarly, the metal grades of zinc-rich stockwork ores (FZ) are too low to warrant commercial extraction. Tin-rich ores were an important source of revenue in the early years of the mine but are now exhausted. They occurred mostly in the lower parts of the Corvo and Graça orebodies (Relvas et al. 2006a,b).

In general, the high tin and base-metal grades of the deposit are accompanied by high concentrations of several by-products, such as selenium and indium (Carvalho et al. 2018). High indium grades can be associated with all ore types, except FE and ME, but preferentially occur in contiguous zones within the copper-rich ores (Carvalho et al. 2018).

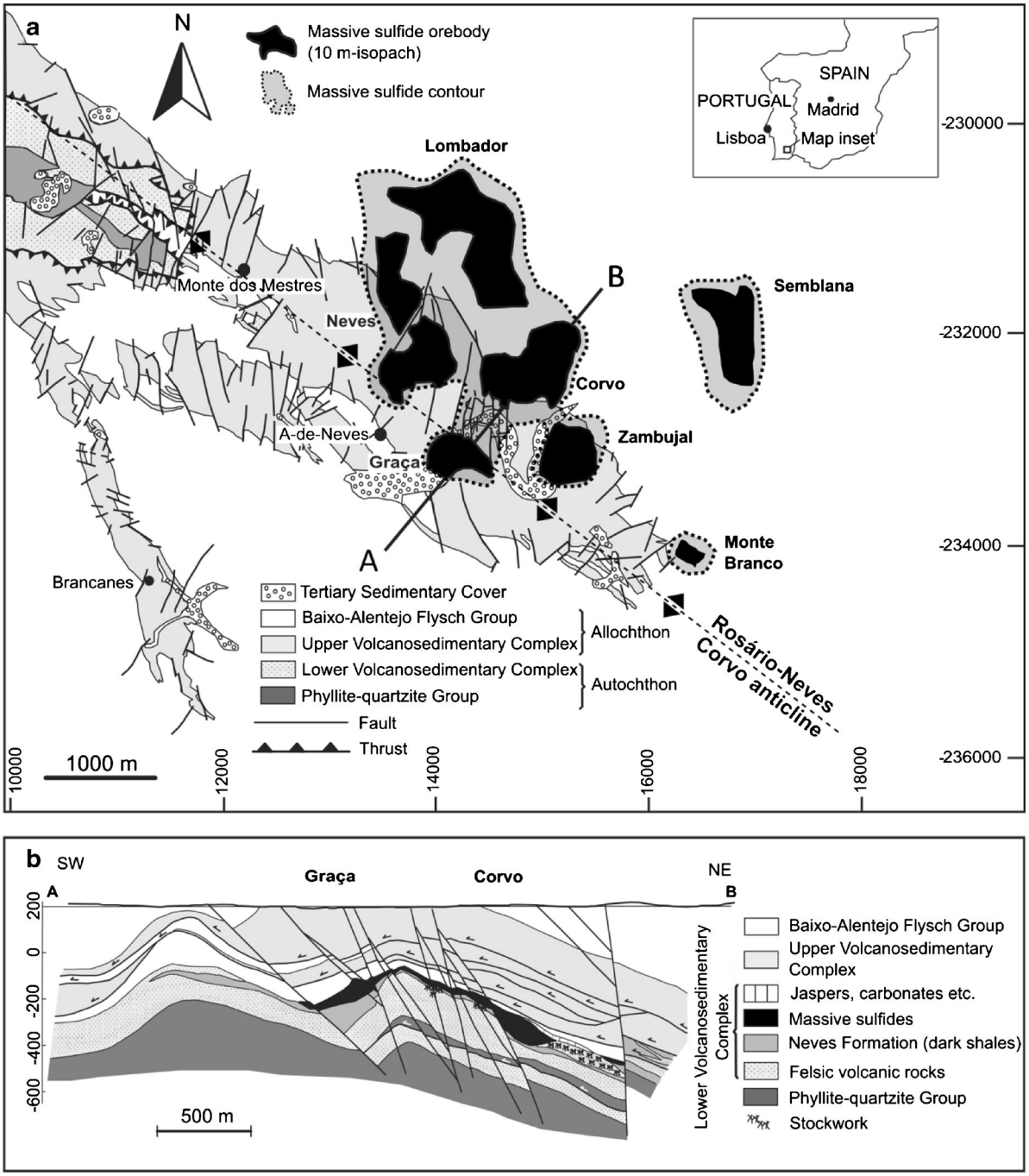

Fig. 1 Geological setting of the Neves-Corvo deposit. Adapted from Relvas et al. (2006a) and Carvalho et al. (2018): **a** map view; **b** cross section (**a**–**b**) through Graça and Corvo ore bodies. Grid references refer to Portuguese National Grid

Materials and methods

The requirements given for deportment studies above (Eq. 1) provide the basis for the general procedure we used to characterize indium deportment in this study. The $\{x_i\}$ were determined using SEM-based image analysis (MLA), while indium concentrations in relevant minerals within each sample were measured using EPMA ($\{c_i\}$). Combining the results from these two techniques yields an estimate of indium deportment for each sample, as well as a calculated bulk indium concentration (C_{In}') (cf. Fig. 3). This is then compared with an independently measured bulk indium concentration (C_{In}) for quality control. Confidence intervals (95%) are estimated for both C_{In} and C_{In}' to facilitate comparison.

Table 1 Overview of ore-type classification at Neves-Corvo

Category	Ore type abbreviation	Full designation	Mean metal grades[a]
Tin-rich ores	FT	Tin-rich stockwork ore	Cu, 1.9%; Zn, 0.4%; Sn, 4.7%
	MT	Massive tin ore	Cu, 7.0%; Zn, 0.7%; Sn, 13.4%
	MS	Copper-rich massive sulfide with economic levels of tin	Cu, 13.0%; Zn, 2.1%; Sn, 1.7%
Copper-rich ores	FC	Copper-rich stockwork ore	Cu, 2.1%; Zn, 0.9%; Pb, 0.5%; Sn, 0.06%
	MC	Copper-rich massive sulfide	Cu, 2.0%; Zn, 0.7%; Pb, 1.2%; Sn, 0.09%
	MCZ	Copper-dominant polymetallic massive sulfide	Cu, 4.2%; Zn, 5.4%; Pb, 0.9%; Sn, 0.07%
Zinc-rich ores	FZ	Zinc-rich stockwork ore	Cu, 0.2%; Zn, 2.3%; Pb, 0.9%; Sn, 0.03%
	MZ	Zinc-rich massive sulfide	Cu, 0.4%; Zn, 6.1%; Pb, 0.5%; Sn, 0.05%
	MZP	Zinc-dominant polymetallic massive sulfide	Cu, 0.4%; Zn, 7.8%; Pb, 2.5%; Sn, 0.05%
Lead-rich ores	MP	Lead-rich massive sulfide	Cu, 0.5%; Zn, 0.1%; Pb, 6.7%; Sn, 0.05%
Barren materials[b]	FE	Barren stockwork ore	Cu, 0.2%; Zn, 0.2%; Pb, 0.1%; Sn, 0.03%
	ME	Barren massive sulfide	Cu, 0.4%; Zn, 0.2%; Pb, 0.3%; Sn, 0.04%

After Gaspar and Pinto (1991), Gaspar (2002), Relvas et al. (2006a, b), and Carvalho et al. (2018)

[a] Compiled from a set of 1668 drill-core analyses for FC, MC, MCZ, FZ, MZ, MZP, MP, FE, and ME ore types, representative of run-of-the-mill ores; values for MT, FT, and MS ore types taken from Gaspar (2002) are mostly of historic interest

[b] Barren materials have Cu, Zn, Pb, and Sn at concentrations below economic levels

The following subsections give further details of sample collection and preparation, the specific analytical methods used, as well as data treatment and final synthesis. Potential difficulties, as well as assumptions made in the data analysis are highlighted in the appropriate sections. A final subsection provides details on the mass balance calculations used to estimate indium recoveries at the mine's processing plants.

Sampling and sample preparation

Two kinds of samples were used in this study:

a) Ore samples collected from underground workings and drill cores ($n = 90$), to study the geological/mineralogical controls on indium deportment in different ore blocks (see Electronic supplementary material (ESM) Tables A1 and A2).
b) Processing samples ($n = 42$) collected from the ore processing plant to study how indium deportment in ores affects its behavior during ore beneficiation (ESM Table A3).

Ore samples were selected based on mineralogical/chemical variability and high bulk indium content (> 10 ppm) as determined on drill core by the mine and on-hand specimens in previous studies (Relvas et al. 2006a; Bachmann et al. 2017). The aim was to cover most major ore types, and thus study the effect of varying modal mineralogy on indium deportment. As noted in ESM Tables A1 and A2, about one third of our samples have already been described elsewhere (Relvas et al. 2006a; Bachmann et al. 2017). Drill core samples were mostly quarter core, > 10 cm in length, while hand specimens were generally larger than 10 × 10 cm, weighing > 500 g each.

Selected ore samples were cut subperpendicular to foliation, as indicated in Fig. 4, to minimize compositional differences between polished sections used for MLA/EPMA analyses, and bulk powder samples used for geochemical analyses. Either polished thick sections (50 × 25 mm) or round mounts (40 mm) were then prepared at the facilities of the Helmholtz Institute Freiberg (HIF). Sample splits for bulk analyses were broken down to subcentimeter size using a steel hammer on a mild steel block, and then ground in an agate ball mill to 100% less than 250 mesh size (0.063 mm) before submission to either in-house or external laboratories.

Processing samples correspond to representative splits (100 g) of monthly composites (> 1 kg) of daily sampling from seven sampling points at each of the two processing plants (Fig. 5) between June and August 2013 (ESM Table A3). For preparation, the sample powders were dried in air at 70 °C, split using a rotary sample divider, and one of the splits (10 g) mixed with graphite powder and epoxy resin to produce one polished grain mount (40 mm round). No sieving was done—grain mounts contained all size fractions. Further splits (90 g) were ground to less than 250 mesh size for geochemical analysis.

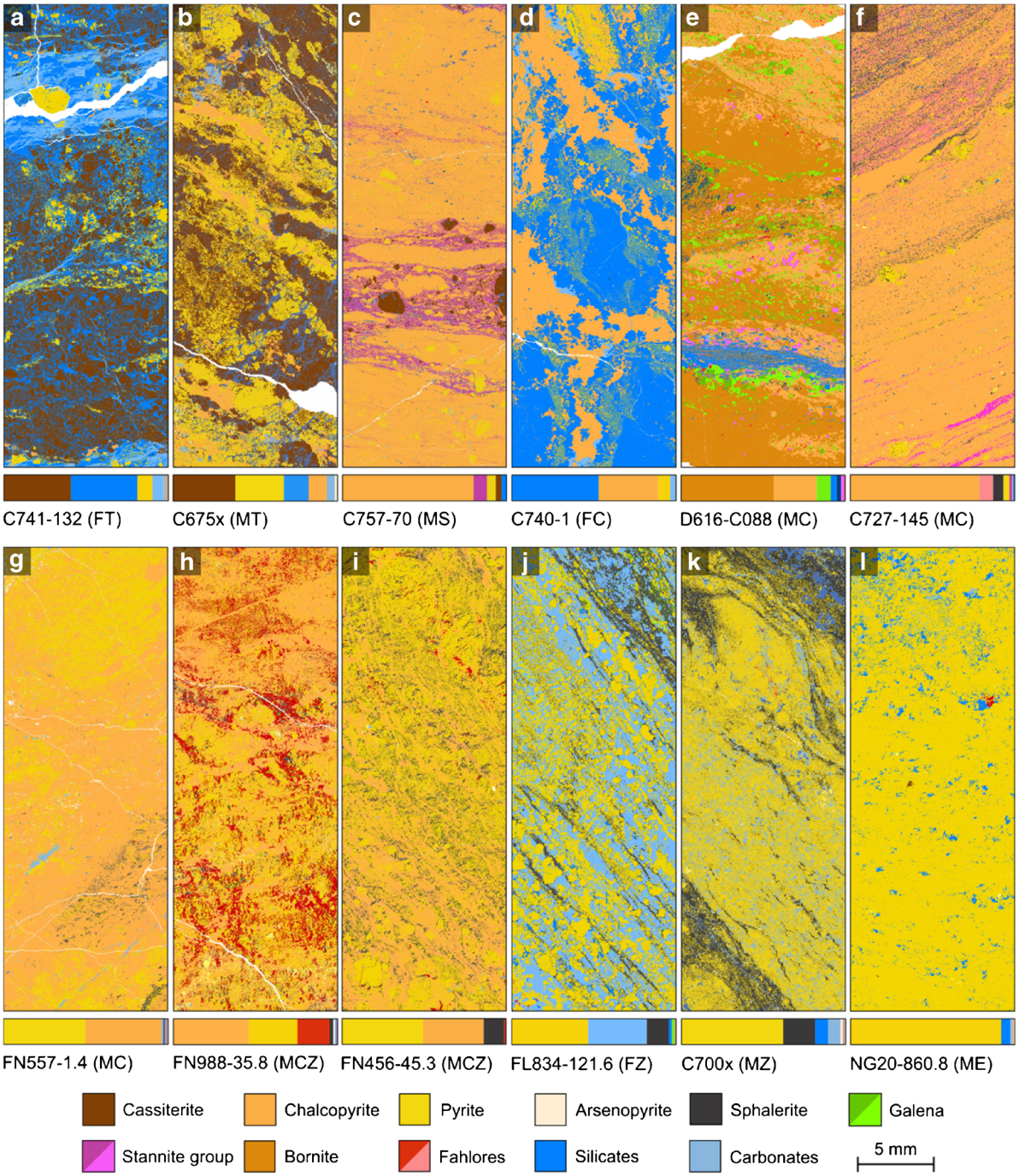

Fig. 2 Mineral maps generated by automated SEM-based image analysis (MLA) for a subset of ore samples, illustrating the range in ore textures and mineralogies covered in this study. The bar diagrams below each mineral map show its modal composition (vol.%). See Table 1 for a detailed explanation of ore-type abbreviations given in brackets behind each sample name

Bulk geochemistry

Several analytical techniques were used to measure the bulk geochemistry of the sample powders: Na_2O_2- and $Na_2B_4O_7$-fusion-inductively coupled mass spectrometry (FUS-ICPMS), instrumental neutron activation analysis (INAA), X-ray fluorescence spectroscopy (XRF), and infrared spectroscopy (IR). Every element was analyzed by at least two different techniques. Analyses were conducted in up to three laboratories: Actlabs in Canada, HIF, and the on-site laboratory of SOMINCOR. Details are provided in the ESM Tables A4–A15. The selection of measured elements includes

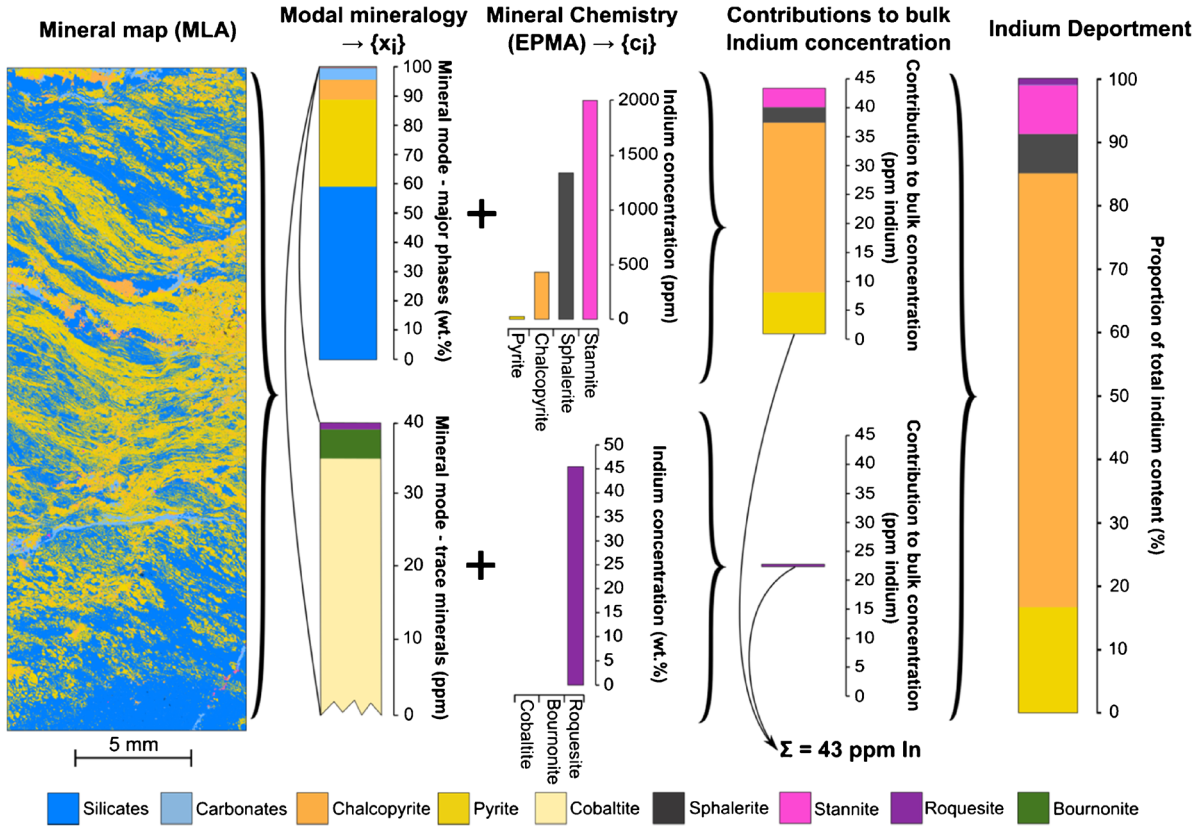

Fig. 3 Schematic representation of methodology used for deportment calculations of ore samples. Modal abundances of both major (top) and trace minerals (bottom) are calculated from a mineral map generated by automated SEM-based image analysis (MLA). Multiplication of these abundances with indium concentrations determined for each mineral by electron-probe microanalysis (EPMA) yields the respective contributions to the overall indium content of the sample, and thus indium deportment (Eq. 1). Data for sample C595-112 (cf. ESM1 Table A1)

all those routinely analyzed on drill core by the mine (i.e., As, Bi, Cu, Fe, In, Pb, S, Sb, Sn, and Zn).

Analyses via different techniques were mostly conducted as consistency checks. In the case of indium, the use of INAA

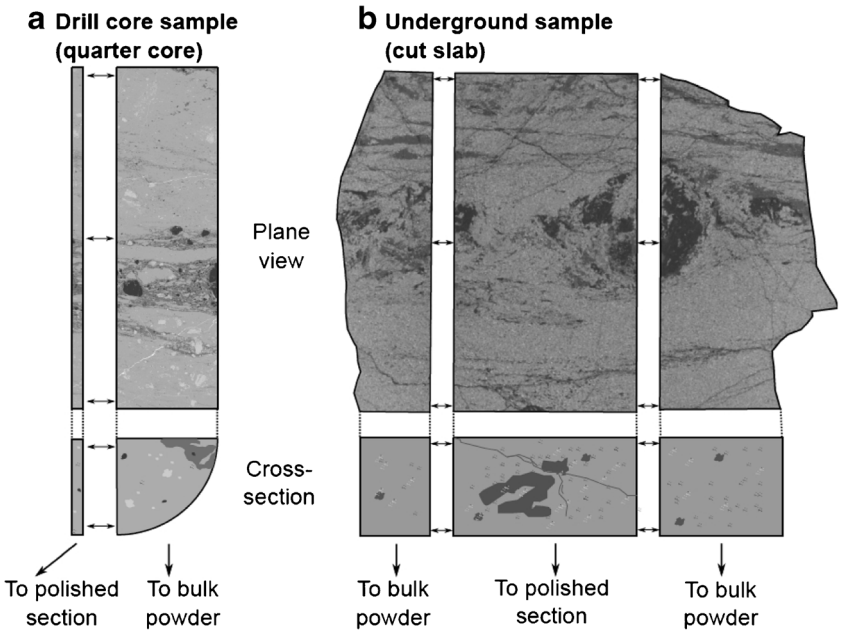

Fig. 4 Schematic diagram of representative splitting of **a** drill-core and **b** underground ore samples to produce polished sections and bulk powders for analysis. Splits were always separated subperpendicular to dominant foliation to avoid systematic differences between powders and sections

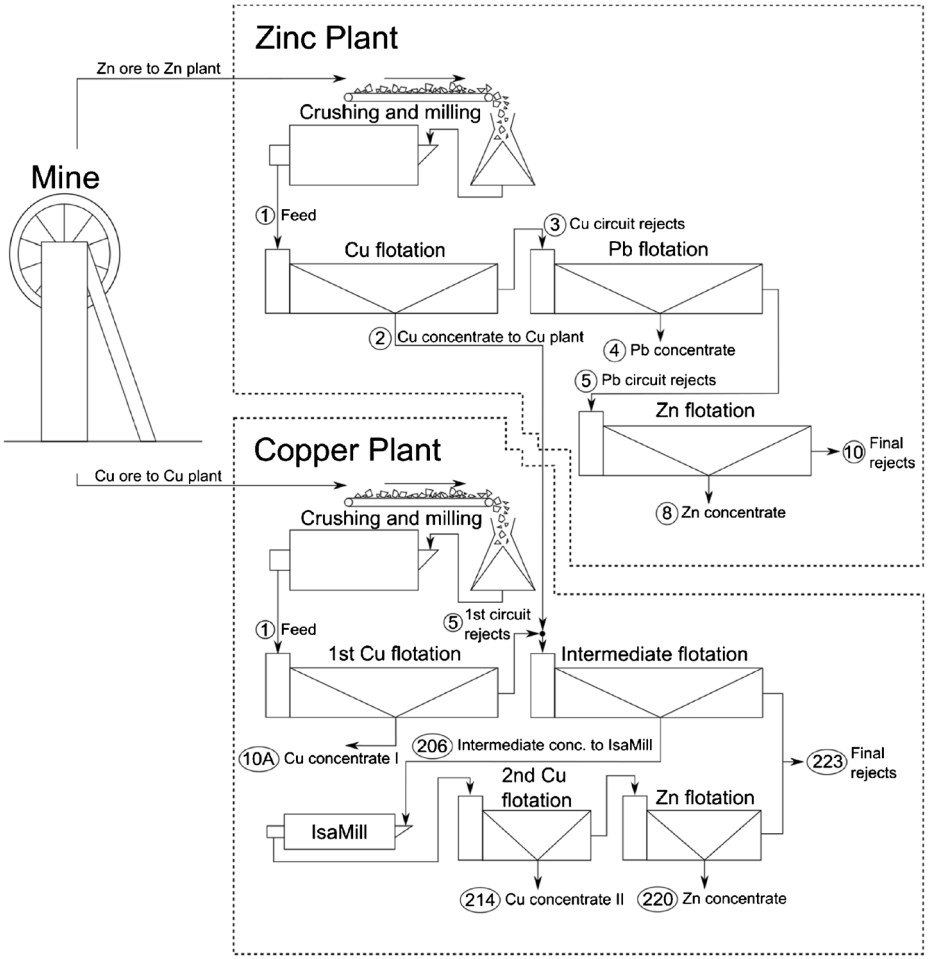

Fig. 5 Schematic overview of the Neves-Corvo processing plants in June to August 2013, showing locations of sampling points (cf. ESM1 Table A3). The plant is subdivided into a copper and a zinc(-copper) part, with respective capacities of 2.5 and 1.0 Mt ore p.a.

was necessary for Sn-rich samples (>> 1 wt.% Sn), due to Sn–In interferences rendering both the XRF and ICPMS techniques unreliable for such samples (cf. Yi et al. 1995; ESM1).

Modal mineralogy (MLA)

Polished sections and grain mounts were carbon coated and measured using the procedures described in Bachmann et al. (2017), to quantify major, minor, and trace mineral abundances (including actual indium minerals). An FEI Quanta 650F SEM equipped with two Bruker Quantax X-Flash 5030 energy dispersive X-ray spectrometers and the MLA software suite, version 3.1.4, was used for data acquisition. The measurements were carried out at HIF. Details of the specific machine settings and measurement parameters are given in Bachmann et al. (2017). More detailed information on the general functionality of the MLA system can be found in Fandrich et al. (2007).

For polished sections, a total area of around 2–5 cm^2 was measured on each sample, while measurements on grain mounts were set up to include between 300,000 and 1,500,000 particles per sample. Higher particle numbers were chosen for samples with lower indium concentrations (i.e., feed, intermediate products and tailings, cf. ESM Table A3).

Electron probe microanalysis

Electron probe microanalysis was performed at HIF with a JEOL JXA 8530F field-emission gun electron microprobe. The machine settings we used and other measurement parameters are described in detail in ESM1. A total of 23 ore samples and 5 processing samples were studied by EPMA, corresponding to 3139 individual spot analyses.

For ore samples, around 20 spots were measured per mineral per sample. In total, 1824 spot analyses were collected on the 23 ore samples. For the processing samples, the focus was on the analysis of chalcopyrite and sphalerite in the copper and zinc concentrates. Between 200 and 250 spot analyses were collected on sphalerite in each of the zinc concentrates, and on chalcopyrite in each of the copper concentrates.

Data treatment

The procedures we used for data treatment served two main purposes: (1) the adjustment of MLA data to reflect compositional differences between polished samples and bulk powders, and (2) the estimation of overall analytical uncertainties. Both are necessary to ensure comparability between bulk geochemistry on the one hand, and MLA/EPMA data on the other. Below, we briefly describe the general principles used for both purposes. Detailed descriptions of the key assumptions, the procedures used for specific data types and the final synthesis are given in ESM1, together with the R-scripts used to implement them.

Adjustment of MLA data

Due to sampling effects, a polished section prepared from a hand specimen or core sample (as used for MLA/EPMA measurements) will not generally have the same bulk composition as the powder sample prepared for bulk geochemistry. Compositional differences may also be present for processing samples due to sedimentation effects that occur during the preparation of grain mounts (Heinig et al. 2015).

To eliminate as much as possible of the effects of such differences on comparisons between calculated (C_{In}') and measured (C_{In}) bulk indium concentrations, we adjusted the modal mineralogy (major minerals) determined by MLA measurements using major element concentrations determined by bulk geochemical analyses (using As, Cu, Fe, Pb, S, Sb, Sn, Zn, but *not* In). This was done using a mode calculation incorporating some of the mineral ratios determined by MLA (ESM1). Similar adjustment procedures are standard in studies of PGE deportment (e.g., Barnes et al. 2008; Osbahr et al. 2014).

Estimation of analytical uncertainties

Analytical uncertainties were estimated using Monte-Carlo-type simulations to propagate known uncertainties on individual measurements through to aggregate quantities, such as calculated bulk indium concentrations and mineralogical deportments. This is the standard approach for uncertainty assessment in many scientific disciplines (e.g., James 1980). Uncertainties were assessed for all input data types (bulk geochemistry, MLA and EPMA data; cf. ESM1) to yield a realistic estimate of aggregate overall uncertainties on the derived quantities.

Mass balance calculations—estimated indium recoveries

The key figure in a discussion of the beneficiation behavior of indium is its recovery in the copper and zinc (and lead) concentrate streams, since this determines how much of it will be available for commercial extraction. A complementary number is the proportion lost to tailings. To calculate these proportions, it is first necessary to establish mass balances for the corresponding process streams. The corresponding procedures are well established in the minerals processing literature (e.g., Chen and Petruk 1980; Petruk and Schnarr 1981) and need not be elaborated here. In our case, the following elements were used for mass-balance calculations: As, Bi, Cd, Cu, In, Pb, Sb, and Zn.

Once mass balances for the different process streams are established, indium recoveries can be estimated by comparing the amount of indium reporting to concentrate streams to the total amount entering the system in feed materials.

Results

The following subsections provide an overview of our analytical results. We first review data quality, followed by the results for ore samples, and then processing samples. The final subsection presents estimates of indium recoveries at the two processing plants.

Data quality

Two critical aspects of data quality are (1) the comparability between measured and calculated bulk indium concentrations (from MLA and EPMA data) and (2) the precision of estimated deportments. A third aspect, the quality of bulk indium analyses is discussed in detail in ESM1 section A7. Bulk indium analyses were generally found to be reliable.

Correspondence between MLA/EPMA and bulk data

A comparison between bulk indium concentrations calculated from MLA/EPMA data and those measured by bulk analytical techniques is shown in Fig. 6. Within error, most samples fall on a 1:1 line. A t test ($p = 0.25$) also demonstrates that there is no statistically significant systematic difference between the two sets of values. Detailed results for each sample can be found in ESM1.

Only one sample lies significantly off the trend—C741-132. This is a very cassiterite-rich and sulfide-poor sample (cf. Fig. 2). If the cassiterite in this sample contained only ~ 10–20 ppm indium, it would also fall within error of the 1:1 line. All other cassiterite-rich samples do fall close to the line. Our assumption that cassiterite contains negligible indium concentrations therefore still appears justified.

Precision of calculated deportments

Monte-Carlo simulations yield a range of plausible representations of the true state of a sample based on the measured data

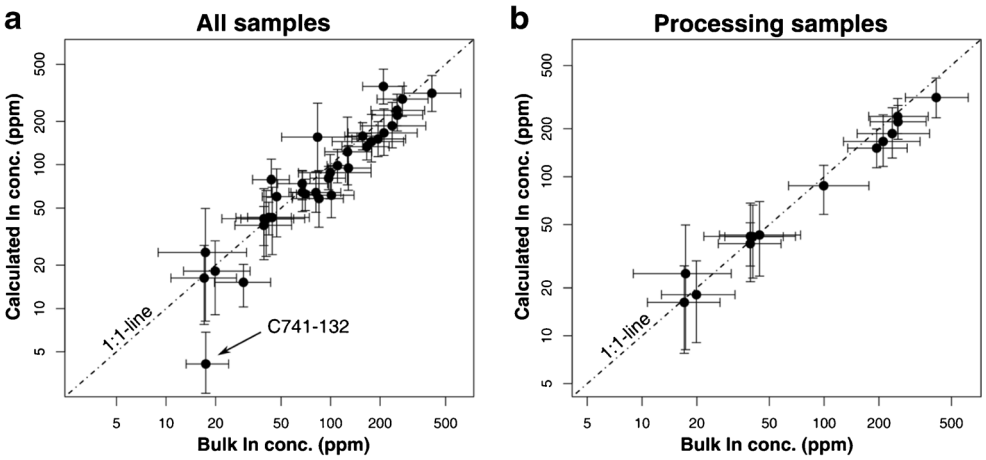

Fig. 6 Correspondence between calculated and measured bulk indium concentrations for **a** all samples investigated in this study and **b** the processing samples only. Note the excellent correspondence between the two sets of values, except for sample C741-132

(e.g., Mariano and Evans 2015). Differences between individual simulation results therefore give an idea of how analytical uncertainties translate to uncertainties in calculated deportments. Before presenting our results in detail, it is necessary to ascertain how large these uncertainties are. To do so, Fig. 7 shows 20 simulation results for one of our samples (FZ552-39.7). This illustrates that qualitative results are very consistent: sphalerite is the most important indium host in 19 out of the 20 simulations (just as in the best estimate shown at the top of the figure), with chalcopyrite as the second, and either stannite or pyrite as the third most important carrier mineral. Simulations for other samples show a similar level of

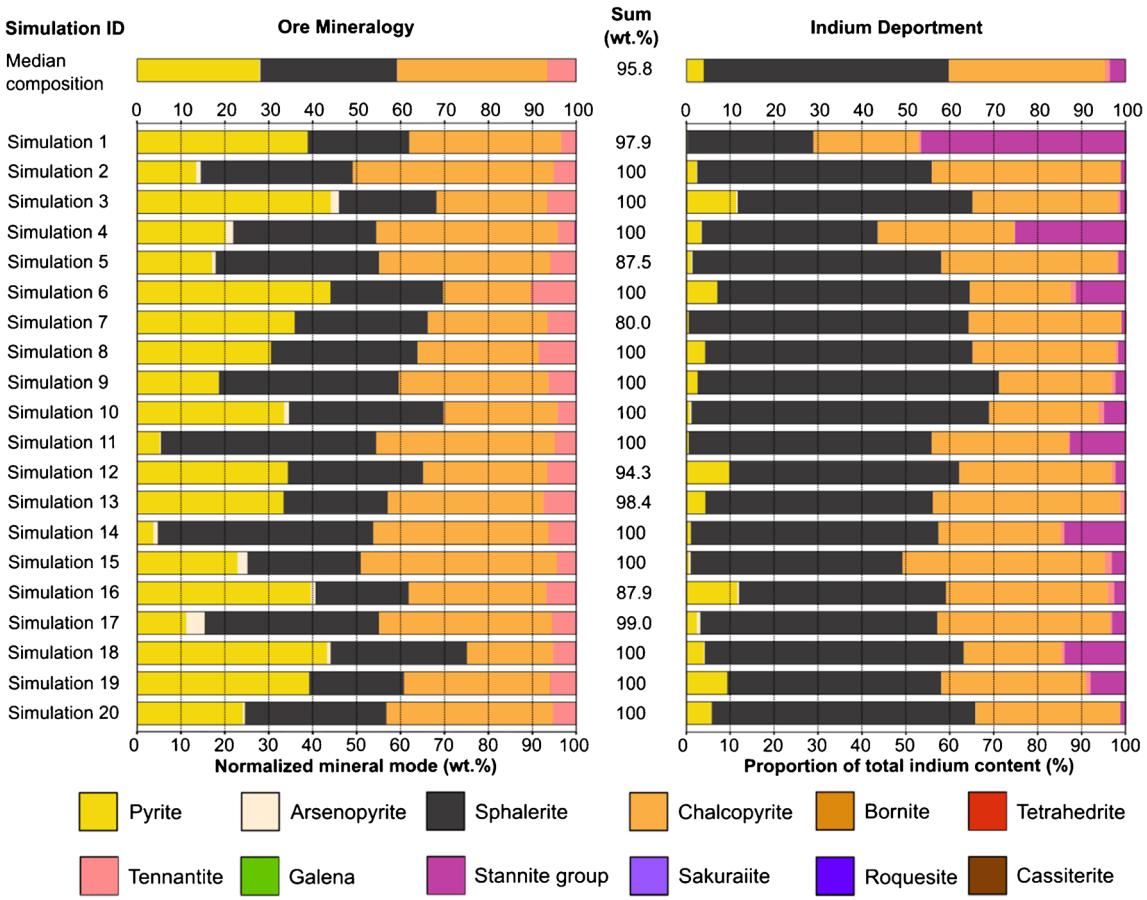

Fig. 7 Variability of simulated deportments for sample FZ552-39.7. The bar diagram at the top shows median composition and deportment. Note that the ore mineralogy plot on the left shows abundances of ore and sulfide gangue minerals normalized to a sum of 100%. Non-sulfide gangue minerals are not shown because they do not contribute to the indium budget of the samples

consistency. However, it is also apparent that there can be considerable uncertainty regarding the exact contributions of different minerals to the overall indium budget of a sample.

Deportment in ores

In this subsection, we first present estimated indium deportments for the 23 ore samples measured by MLA and EPMA. We then explore the regularities in the partitioning of indium between the main ore minerals (mostly sphalerite, chalcopyrite and the stannite group minerals), as well as the occurrence of indium minerals in our samples, in more detail.

Estimated deportments

Figure 8 shows estimated indium deportments for the 22 selected ore samples and the barren pyritic sample. The Sn-rich ores are shown at the top, the Cu-rich ores in the middle, and the more Zn-rich ores towards the bottom of the figure. The "barren" massive sulfide sample analyzed in this study is shown at the very bottom. Note that samples are sorted by ascending sphalerite-to-chalcopyrite ratio within ore types to show systematic changes in deportment with ore mineralogy.

It is clear from Fig. 8 that chalcopyrite and sphalerite are the most important indium carriers in all ore types. Furthermore, the relative proportions of indium hosted by these two minerals correlate closely with their relative abundances. In contrast with chalcopyrite and sphalerite, the stannite group minerals, the indium minerals roquesite and sakuraiite, pyrite, and other sulfides account for less than half of the total indium content in the studied samples. This is particularly true for the Cu- and Zn-rich ores. However, it should be noted that average pyrite content in the ore samples shown in Fig. 8 is somewhat lower than in average run-of-the-mill ores (see section on processing samples). This is due to the preferential selection of more indium-rich materials for analysis. These materials tend to have less pyrite. Pyrite unsurprisingly appears to be a more important host in more pyrite-rich materials (e.g., samples C700x and NK22A-1075.2), but still only accounts for less than half of all indium in current run-of-the-mill copper and zinc feed (see below).

In the Sn-rich ores, the stannite group minerals, together with the indium minerals, may account for up to 40% of the total indium content, while pyrite can account for up to 30%. Particularly, the cassiterite-rich samples tend to have higher proportions of indium in stannite and the indium minerals. The only other sample with a significant percentage of indium in roquesite is D616-C088. This sample is unusual in terms of its modal mineralogy, however, with bornite rather than chalcopyrite as the dominant copper-iron-sulfide mineral, and virtually no sphalerite and pyrite. Bornite is a relatively rare

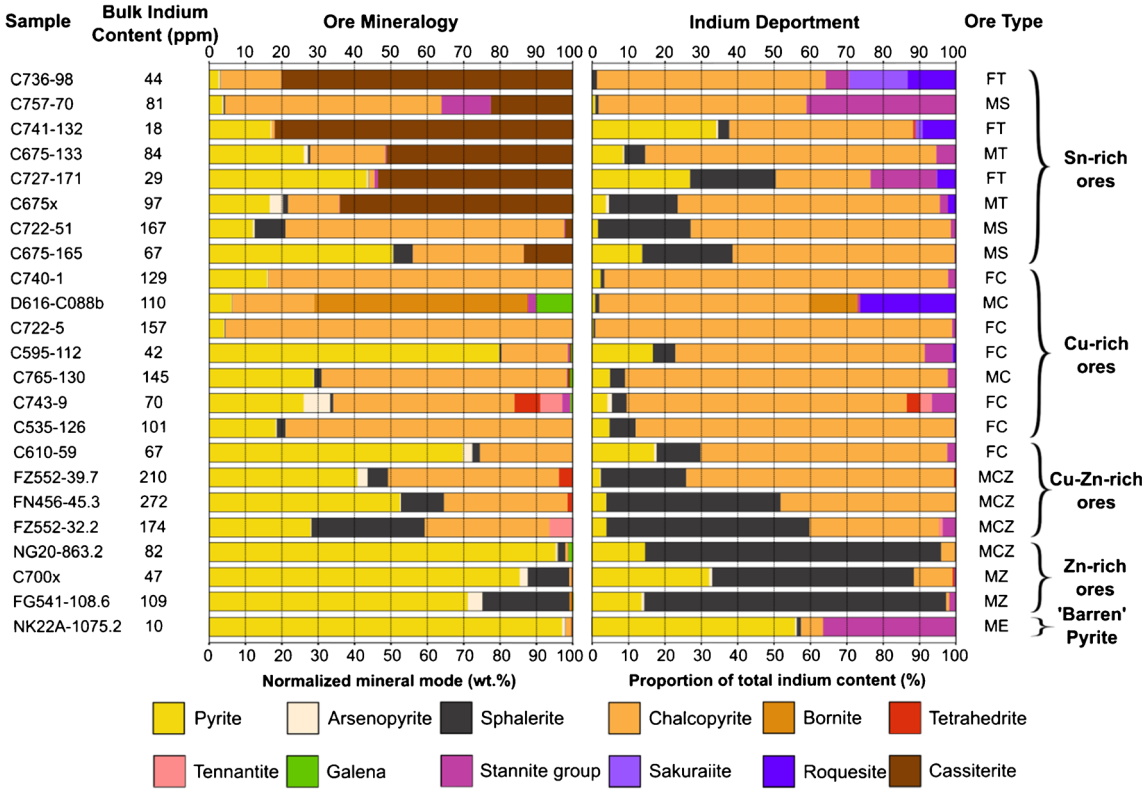

Fig. 8 Indium deportment in ore samples. Note that the ore mineralogy plot on the left shows abundances of ore and sulfide gangue minerals normalized to a sum of 100%. Non-sulfide gangue minerals are not shown because they do not contribute to the indium budget of the samples

mineral at Neves-Corvo and only occurs in significant quantities in isolated parts of the deposit (Gaspar 2002).

Partitioning of indium between major host phases

The correlation of indium deportment with modal mineralogy, particularly for sphalerite and chalcopyrite, suggests that some regularity is present in its distribution across different minerals. The extent of these regularities is explored further in Fig. 9. The partitioning coefficients used in this figure are defined as:

$$D_{i-j} = \frac{c_i}{c_j} \quad (2)$$

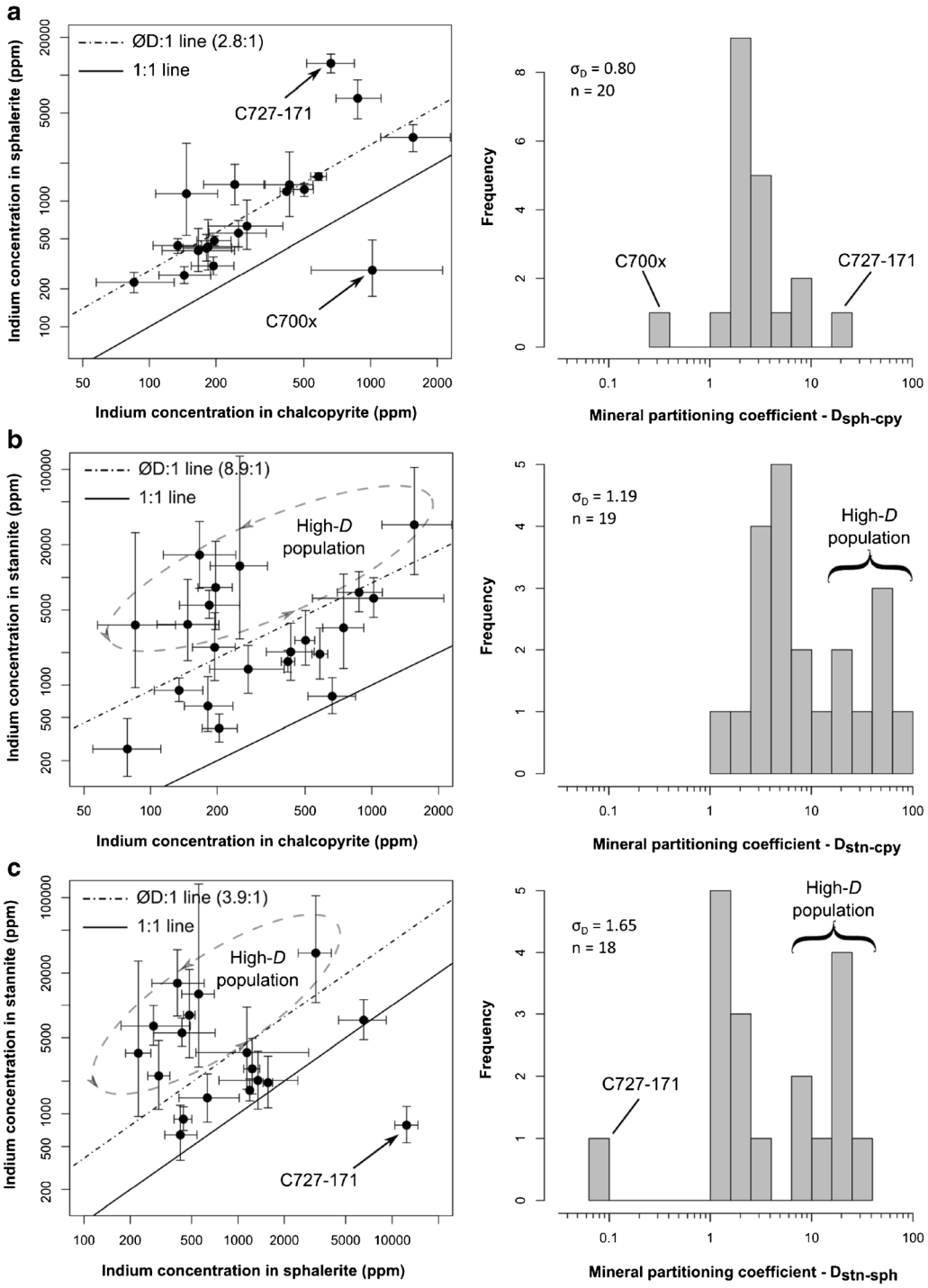

Fig. 9 Partitioning behavior of indium between different mineral pairs in Neves-Corvo samples: **a** chalcopyrite–sphalerite, **b** chalcopyrite–stannite, and **c** sphalerite–stannite. See text for further comments

where c_i and c_j are the (arithmetic) mean indium concentrations in minerals i and j within a sample. We use the arithmetic mean, since we are mostly interested in process-relevant data in this work (beneficiation), and therefore mass balances. We note, however, that the geometric mean would be more appropriate for considerations concerning the central tendency of a population approximately following a log-normal distribution (cf. van den Boogaart and Tolosana-Delgado 2013).

The standard deviation (σ_D) given with the histograms in Fig. 9 is the log-standard deviation of the D_{i-j}. This provides a direct measure of the width of the distributions. It is clear from these values that the spread of D values is smallest for the pair sphalerite–chalcopyrite, for which most samples fall on a linear trend in the corresponding scatterplot (Fig. 9a). Furthermore, the histogram shows a single peak, suggesting a roughly log-normal distribution, with D values ranging from 0.3 to 19 (Fig. 9a). The geometric mean of these values is ~ 2.8. Indium concentrations in sphalerite are generally higher than in coexisting chalcopyrite. Only one sample deviates from this trend, C700x. This is the only sample where the measured mean indium concentration in chalcopyrite is higher than in sphalerite. The other sample with an extreme D value is C727-171, with $D_{\text{sph-cpy}} = 19$.

For the pair stannite–chalcopyrite, the D values show a greater spread than for sphalerite–chalcopyrite (Fig. 9b). In fact, two parallel trends appear to be present on the scatterplot, one corresponding to higher D values (10–100, gray ellipse), the other to lower ones (1–10). This is also reflected in the histogram, showing two peaks rather than one (Fig. 9b). Thus, there seem to be two populations of samples according to how indium partitions between stannite and chalcopyrite. Irrespective of these complexities, the indium concentration in stannite is always significantly higher than in coexisting chalcopyrite. The overall geometric mean of $D_{\text{stn-cpy}}$ is 8.9. Means for the two subpopulations are around 5 and 30, respectively, depending where the dividing line is drawn.

The data for stannite–sphalerite shows a similar overall structure to the stannite–chalcopyrite data (Fig. 9c). That is, there also seem to be two populations, one with higher D values (6–40) and one with lower ones (1–4). These are visible in both the scatter-plot and histogram. Indium concentrations in stannite are higher than in co-existing sphalerite, except for one sample, C727-171. The geometric mean of $D_{\text{stn-sph}}$ is 3.9. Means for the two subpopulations are around 2 and 20, respectively.

For other sulfide minerals (pyrite, arsenopyrite, fahlores, bornite), indium partitioning behavior could not be reliably assessed due to low concentrations. However, assuming mean concentrations of 25 ppm for these minerals in all samples, rough estimates of the means of the corresponding mineral partitioning coefficients can still be compiled. For pyrite, the results are: $D_{\text{cpy-py}} = 12$, $D_{\text{sph-py}} = 34$, and $D_{\text{stn-py}} = 110$. Essentially, the same values would result for arsenopyrite, tetrahedrite, etc.

As a last important point, it should be noted that the values of the partitioning coefficients considered in this section appear to be completely unrelated to the different ore types described earlier (Table 1).

Occurrence of indium minerals

Just like the partitioning of indium between certain major and minor ore minerals, the occurrence of discrete indium minerals (roquesite and sakuraiite) also follows a regular trend. This is shown in Fig. 10a. In this figure, the proportion of indium hosted in discrete indium minerals is plotted against model indium concentration in sphalerite for each sample. We use model concentrations rather than measured values to be able to include all samples with MLA and bulk geochemistry data not just those for which EPMA data had also been collected.

The sphalerite model concentration was calculated as follows, using the mean mineral partitioning coefficients determined in the previous subsection (Fig. 9):

$$c_{\text{sph}}^{\text{Model}} = \frac{C_{\text{In}} - 25\ \text{ppm} \times \left(x_{\text{py}} + x_{\text{aspy}} + x_{\text{tn}} + x_{\text{tetr}} + x_{\text{bn}}\right)}{\left(x_{\text{sph}} + \frac{x_{\text{cpy}}}{D_{\text{sph-cpy}}} + D_{\text{stn-sph}} \times x_{\text{stn}}\right)} \quad (3)$$

where C_{In} is the bulk indium concentration in the sample, and x_i is the modal abundance of mineral i. Mineral abbreviations used in this formula are py for pyrite, aspy for arsenopyrite, tn for tennantite, tetr for tetrahedrite, bn for bornite, sph for sphalerite, cpy for chalcopyrite, and stn for stannite. A similar model indium concentration can be calculated for chalcopyrite.

Figure 10b and c show that these model concentrations correlate very well with measured concentrations in most samples. Outliers are those samples which had already been identified as unusual in the previous subsection.

Even though the overall trend is very broad, it is nevertheless clear from Fig. 10c that the proportion of indium hosted in roquesite and sakuraiite increases rapidly with the indium concentration in sphalerite. The abundances of these minerals only reach measurable levels in samples where the indium concentration in sphalerite exceeds a minimum of around 500 ppm. However, for samples with an indium concentration of more than 2000 ppm in sphalerite, a sizeable proportion of the overall indium content is expected to be hosted in indium minerals. Again, the observed behavior appears to be independent of ore type.

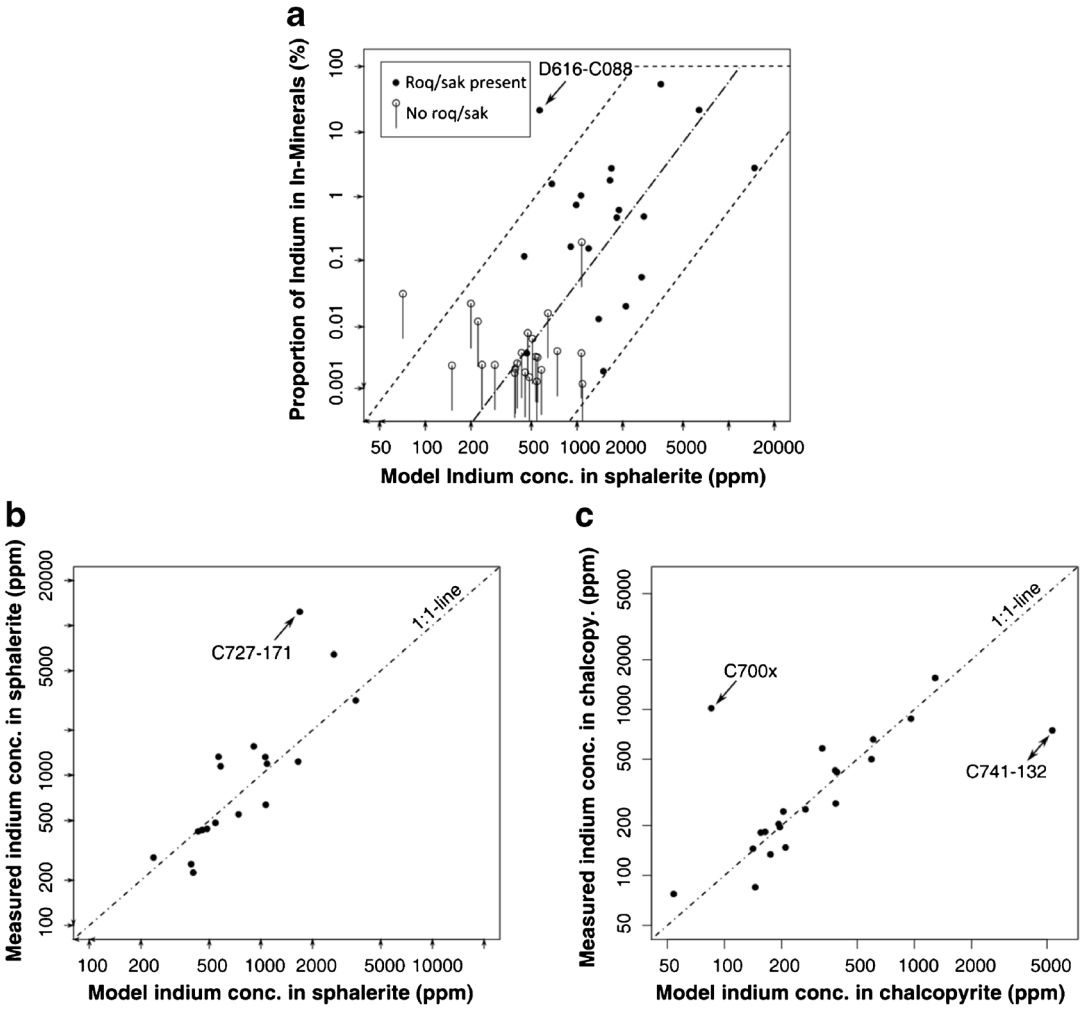

Fig. 10 Occurrence of indium minerals in Neves-Corvo samples: **a** correlation of abundance with model indium concentration in sphalerite; **b** reliability of model indium concentrations calculated for sphalerite; and **c** for chalcopyrite. For samples in (**a**) which do not contain indium minerals, the detection limit of the MLA is shown

Mineralogical deportment in mill feed and beneficiation products

Figure 11 summarizes estimated indium deportments for mill feed, beneficiation products, and intermediate process streams at the zinc and copper plants in June 2013 and illustrates the relative magnitudes of different process streams derived from mass balance calculations (see following section for detailed results).

As expected from the analysis of ore samples, sphalerite and chalcopyrite combined are the most important indium carriers in the feed materials of both plants (Cu and Zn ores), accounting for ~ 55–70% of the total indium content. The second most important carrier mineral is pyrite (~ 20–40% of total indium). Stannite and the indium minerals, on the other hand, are only of minor importance, accounting for less than 10% of the total indium content in the feed. This is in good general agreement with the results from individual ore samples presented above. However, the importance of pyrite is relatively high in the feed materials compared with the investigated ore samples. This is because the feed materials have higher pyrite contents (cf. Fig. 8).

While sphalerite and chalcopyrite are also the most important indium carriers in all concentrate streams (75–95%), pyrite dominates in the final rejects (~ 50–70%). Stannite and the indium minerals remain of relatively minor importance in all final outputs (< 20%; stream (2) at the Zn plant is not a final output). They generally follow the ore minerals, particularly chalcopyrite, into the various concentrate streams.

Differences between the two processing plants are mostly related to differences in the mineralogical (and mineral-chemical) compositions of the feed materials. For instance, chalcopyrite is more important as an indium carrier in the copper plant, simply because the feed material contains much

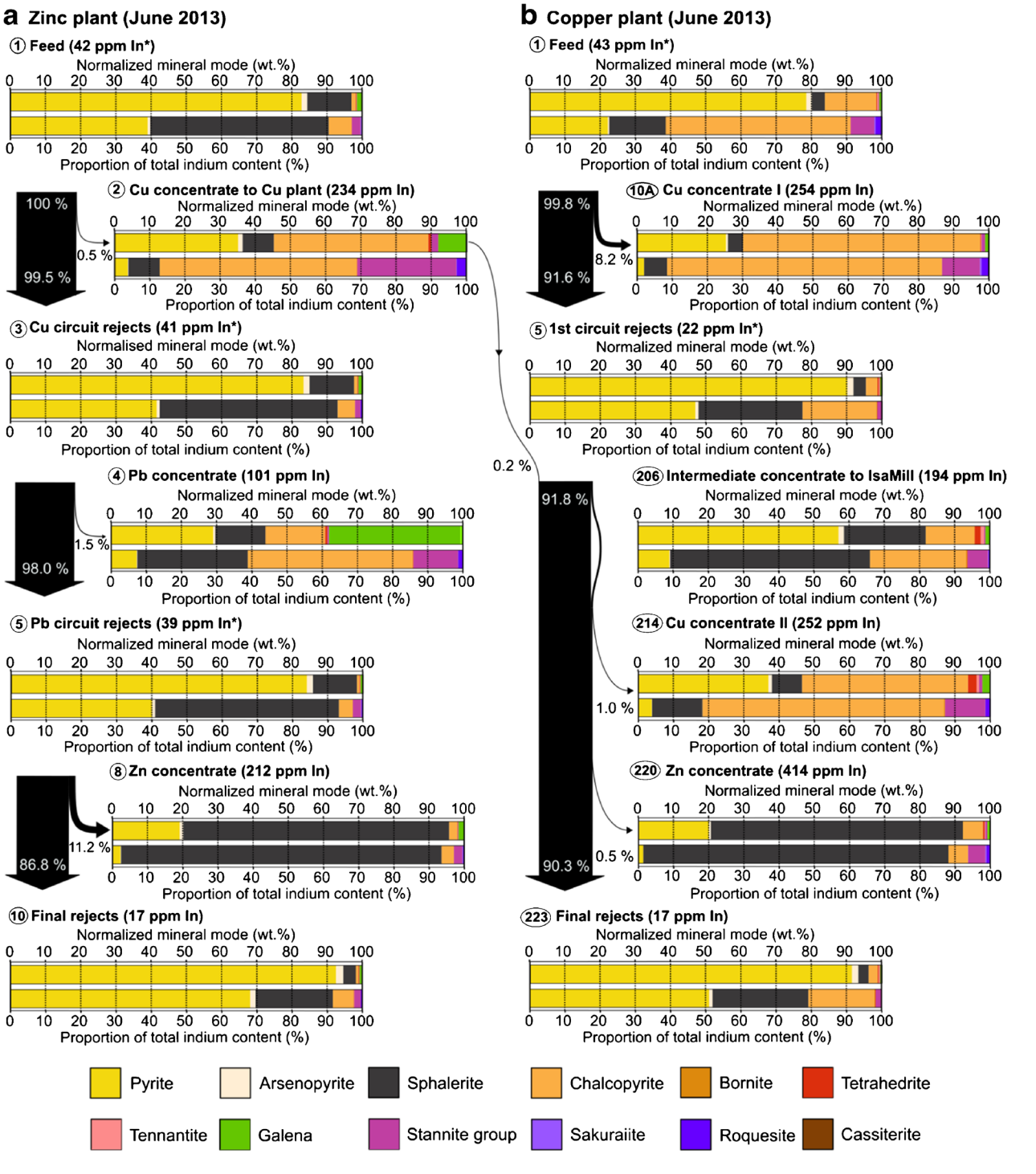

Fig. 11 Indium deportment in processing samples of **a** the zinc plant and and **b** the copper plant from June 2013. For each sample, the upper bar diagram shows its mineralogical composition (sulfides and cassiterite only, as in Figs. 7 and 8), and the lower one shows the mineralogical deportment of indium. Arrows indicate the direction and relative magnitudes of mass flows within each processing plant

more of it. Similarly, the proportion of indium associated with pyrite is less in the rejects of the copper plant, because there is slightly less pyrite (and more chalcopyrite and sphalerite) in this material than the rejects of the zinc plant, but also because average indium concentrations in chalcopyrite and sphalerite at the copper plant are higher than they are in the zinc plant, as is apparent from the absolute indium concentrations of the copper and zinc concentrates of both plants.

Indium recovery at the processing plants

Table 2 provides an overview of the results of mass balance calculations for relevant process streams (feed, concentrates, and final rejects). This table also includes best estimates of indium concentrations, as well as modal abundances of sphalerite, chalcopyrite and pyrite for each sample. Using this information, we estimated how each of these four components reports to different process streams. These estimates are shown in the right-hand part of the table. The sum of the percentages reporting to different concentrate streams is equal to the overall recovery, while the percentage reporting to the final rejects is lost to tailings.

It is apparent from Table 2 that 45–65% of the indium entering each processing plant (52–64% overall, i.e., both plants together) is recovered in the various (payable) concentrate streams. This compares with recoveries of 83–88% for chalcopyrite (Cu) at the copper plant (81–86% overall) and recoveries of 75–85% for sphalerite (Zn) at the zinc plant (70–75% overall). The recoveries of these ore minerals are clearly higher than those of indium. This is explained by the substantial portion of indium entering both processing plants in, or associated to, pyrite (~ 20–40%; cf. Fig. 11). As the main sulfide gangue mineral, pyrite reports almost exclusively to the final rejects (92–95%). Thus, virtually all indium associated with pyrite is lost to the tailings. This is compounded by the indium contained in the lost fractions of sphalerite and chalcopyrite, suppressing overall indium recoveries significantly below the levels of sphalerite (zinc) and chalcopyrite (copper).

Discussion

Prediction of indium deportment and recovery from bulk geochemistry

Two steps are necessary to predict indium deportment from a bulk geochemical assay. First, a modal mineralogy needs to be derived, and second, indium needs to be distributed across the different minerals according to its expected partitioning behavior.

Modal mineralogy

A procedure for the calculation of modal mineralogy from bulk assays must necessarily be based on assumptions on the relative abundances of certain minerals, as well as their composition (cf. ESM1 section A6.2). Since the tin ores are already exhausted, it is sufficient for such a procedure to produce reliable results for the copper and zinc ores that are currently exploited. The most important indium carriers in these ores are sphalerite, chalcopyrite, and pyrite. Minor minerals are not of major importance according to the results presented earlier.

Based on our data, the following simplifying assumptions are possible:

1) The stannite-to-cassiterite ratio can be assumed to be constant. Neither stannite nor cassiterite are particularly abundant in currently produced ores (average concentrations < 0.1 wt.%) and do not account for a major proportion of the indium hosted in these ores (< 10%; cf. Figs. 8 and 11).
2) The concentrations of bournonite, tennantite, cobaltite, and clausthalite can be assumed to be zero, such that all Sb is hosted by tetrahedrite, all As by arsenopyrite, and all Pb by galena. None of these minerals are generally relevant hosts of indium due to their low overall abundances and generally low indium concentrations.
3) Bornite concentrations can be assumed to be zero unless the corrected Cu/Fe ratio of the sample (after subtracting the Cu associated to tetrahedrite and stannite) is > 1.1 by weight.

Based on these assumptions, the modal mineralogy can be estimated according to the modified procedure described in ESM1 section A6.5.

Figure 12 provides a comparison between the results from this simplified calculation and those for the more complex procedure described in ESM1 section A6.2, for relevant samples (copper, zinc, and "barren" ores). The general agreement between the two sets of results is clearly very good, validating our approach. However, there are also some differences due to the simplifying assumptions we made. For instance, tennantite-containing samples (C743-9 and FZ552-32.2) are predicted to have significantly more arsenopyrite, since tennantite is not considered in our calculation. However, these differences have a negligible effect on predicted indium deportments.

Indium deportment

Once a modal mineralogy is established, the mineralogical deportment of indium can be estimated as follows, using its average mineral partitioning behavior:

1) Calculate a model indium concentration for pyrite using the mean mineral partitioning coefficients estimated earlier:

$$c_{\mathrm{py}}^{\mathrm{Model}}(\mathrm{In}) = \frac{C_{\mathrm{In}}}{\left(c_{\mathrm{aspy}} + c_{\mathrm{py}} + c_{\mathrm{tetr}} + c_{\mathrm{bn}} + 12 \times c_{\mathrm{cpy}} + 34 \times c_{\mathrm{sph}} + 110 \times c_{\mathrm{stn}}\right)} \quad (4)$$

This equation is analogous to (3) above. If $c_{\mathrm{py}}^{\mathrm{Model}}(\mathrm{In}) \geq 50$ ppm, set indium concentration in pyrite to 50 ppm, otherwise take the value from (4). This more complex

Table 2 Estimated mass flows for ore processing plants and corresponding recoveries (June to August 2013)

Sample	Sample material	In (ppm)	Sph (wt%)	Cpy (wt%)	Py (wt%)	Relative mass flow (%)	Pct. total indium (%)	Pct. total sph (%)	Pct. total cpy (%)	Pct. total py (%)
Cu-06-1	Feed	43.0[b]	2.03[b]	7.18[b]	34.1[b]	99.8[a]	98.9	99.1	98.8	99.8
Cu-06-10A	Cu concentrate I	254.0	4.26	67.4	25.7	8.7	51.4	17.6	81.4	6.6
Cu-06-214	Cu concentrate II	252.0	8.72	47.5	36.5	0.8	4.7	3.3	5.3	0.9
Cu-06-220	Zn concentrate	414.0	72.8	5.78	19.9	0.8	7.7	27.7	0.6	0.5
Cu-06-223	Final rejects	17.0	1.13	0.99	35.0	89.8	35.5	48.3	12.3	92.2
Cu-07-1	Feed	38.0[b]	1.84[b]	5.66[b]	26.1[b]	99.5[a]	98.5	99.1	97.7	99.1
Cu-07-10A	Cu concentrate I	284.0	5.38	66.7	26.2	(6.5)	(48.2)	(19.0)	(76.1)	(6.5)
Cu-07-214	Cu concentrate II	260.0	7.58	54.6	33.6	(0.6)	(4.1)	(2.5)	(5.7)	(0.8)
Cu-07-220	Zn concentrate	438.0	70.8	5.93	23.2	(0.6)	(6.9)	(23.1)	(0.6)	(0.5)
Cu-07-223	Final rejects	17.0[c]	1.11[c]	1.04[c]	26.1	(92.2)	(40.9)	(55.6)	(17.3)	(92.2)
Cu-08-1	Feed	37.0[b]	1.77[b]	6.26[b]	25.7[b]	99.8[a]	98.8	99.2	99.0	99.6
Cu-08-10A	Cu concentrate I	255.0	5.06	71.5	21.9	7.0	47.0	19.8	79.4	6.0
Cu-08-214	Cu concentrate II	256.0	10.1	56.9	30.5	0.4	2.7	2.3	3.6	0.5
Cu-08-220	Zn concentrate	379.0	74.9	4.1	24.9	0.5	5.0	20.9	0.3	0.5
Cu-08-223	Final rejects	18.0	1.09	1.09	26.0	92.1	43.6	56.1	15.9	93.2
Zn-06-1	Feed	42.0[b]	11.5[b]	1.37[b]	63.5[b]	100.0	100.0	100.0	100.0	100.0
Zn-06-2	Cu concentrate	234.0	8.76	43.7	33.3	0.5	2.8	0.4	15.6	0.3
Zn-06-4	Pb concentrate	101.0	14.4	17.0	28.2	2.2	5.3	2.8	26.7	1.0
Zn-06-8	Zn concentrate	212.0	77.6	2.41	19.1	11.3	57.0	76.3	19.5	3.4
Zn-06-10	Final rejects	17.0	2.73	0.59	70.4	86.0	34.8	20.4	36.2	95.3
Zn-07-1	Feed	46.0[b]	14.4[b]	1.20[b]	63.7[b]	100.0	100.0	100.0	100.0	100.0
Zn-07-2	Cu concentrate	166.0	7.95	26.7	48.0	0.4	1.4	0.2	8.9	0.3
Zn-07-4	Pb concentrate	84.0	13.4	12.7	39.2	2.1	3.8	2.0	22.2	1.3
Zn-07-8	Zn concentrate	200.0	81.3	2.06	20.7	13.6	59.1	76.8	23.3	4.4
Zn-07-10	Final rejects	20.0	3.65	0.65	71.4	83.9	36.5	21.3	45.4	94.0
Zn-08-1	Feed	49.0[b]	11.0[b]	1.18[b]	65.6[b]	100.0	100.0	100.0	100.0	100.0
Zn-08-2	Cu concentrate	223.0	7.67	30.3	47.6	0.6	2.7	0.4	15.2	0.4
Zn-08-4	Pb concentrate	70.0	10.7	13.5	37.2	1.4	2.0	1.4	15.8	0.8
Zn-08-8	Zn concentrate	185.0	75.2	1.74	25.0	10.7	40.4	73.1	15.5	4.1
Zn-08-10	Final rejects	31.0	3.11	0.71	71.1	87.3	55.2	24.7	51.7	94.6

[a] Smaller than 100% since total mass-flow to copper plant is supplemented by Cu concentrate from zinc plant

[b] Values recalculated from output materials to achieve consistency. See ESM1 Table A3 for measured indium concentrations for comparison

[c] Mean of values for June and August 2013, since actual sample probably contaminated, cf. Table A3. Mass balance values for July are in brackets, since they were calculated based on average mass flows for June/August, and corrected values for sample Cu-07-223

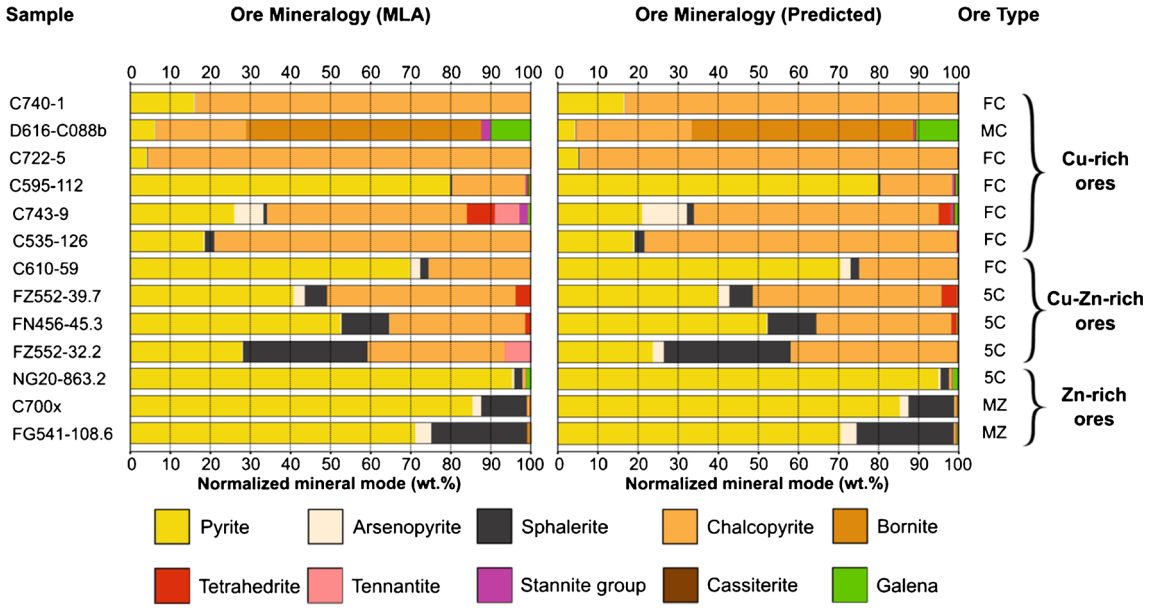

Fig. 12 Comparison between ore mineralogy calculated from MLA measurements and bulk geochemistry (left) as well as ore mineralogy predicted from bulk geochemistry alone (right). See ESM1 section A5 for the detailed procedure. Note good agreement between the two datasets

estimation routine for indium in pyrite (rather than taking an average concentration of 25 ppm as for deportment estimation from EPMA/MLA measurements, cf. ESM1) is necessary to deal with samples having low indium grades (< 25 ppm).

1) Assume the same indium concentration as in pyrite for arsenopyrite, tetrahedrite and bornite, if present.
2) Subtract indium hosted in these minerals from overall indium content, and distribute remainder over sphalerite, chalcopyrite and stannite using the mean partitioning coefficients determined previously.
3) Estimate the proportion of indium hosted in indium minerals (roquesite and sakuraiite) using the relationship between model indium concentration in sphalerite and indium mineral abundance determined previously.
4) Rescale indium concentrations in sphalerite–chalcopyrite–stannite and pyrite–arsenopyrite–tetrahedrite–bornite to reflect the estimated proportion of indium hosted in indium minerals.

Figure 13 provides a comparison between indium deportments predicted according to this procedure, and those measured on samples of copper and zinc ores. Again, there is very good general agreement between the two datasets. Differences arise mainly for the proportion of indium hosted in indium minerals (sakuraiite and roquesite). This is due to the relatively poorly constrained relationship between model indium concentrations in sphalerite and chalcopyrite and the abundance of these minerals (cf. Fig. 10). Differences in the importance of pyrite (particularly samples NG20-863.2 and C700x) result from the modified estimation of indium concentrations in this mineral (eq. (4)).

Recovery

Using estimated deportments, as well as the known behavior of the carrier minerals in the processing plants (Table 2; ESM1 Table 25A), the recoverable fraction of indium can be predicted for each sample. This information is included in Fig. 13. Note that these recoveries are generally somewhat higher than those observed on zinc/copper feed materials (Table 2, Results section) due to the low pyrite contents of these samples.

To better illustrate the dependence of indium recovery on mineralogical composition and indium content of the ores, we also predicted indium recoveries for a representative set of 1231 drill core analyses from the mine database, including 364 samples of copper ores and 867 samples of zinc ores. Data was available for As, Cu, Fe, Pb, S, Sb, Sn, Zn, and In, measured on crushed and homogenized 1-m intervals of core. This allowed us to predict modal mineralogy, deportment and estimated indium recovery for each sample. A summary of selected results is shown in Fig. 14.

While there is only a weak dependence of predicted recovery on indium grade (left-hand panels in Fig. 14), the mineralogy of the ores (right-hand panels), is clearly expected to have a major effect. As discussed before, the non-recoverable fraction of indium is mostly determined by the proportion associated to pyrite, as evidenced by the

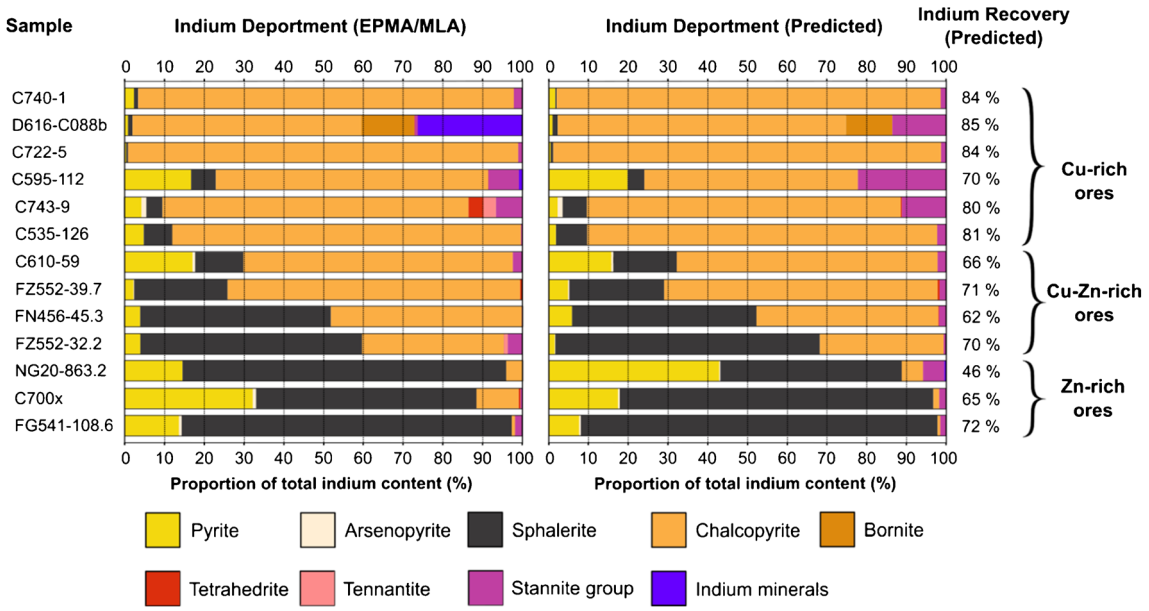

Fig. 13 Comparison between indium determined from MLA/EPMA measurements and bulk geochemistry (left) and indium deportment predicted from bulk geochemistry alone (right) for the same samples as in Fig. 12. See main text for detailed procedure. Note excellent agreement between the two datasets

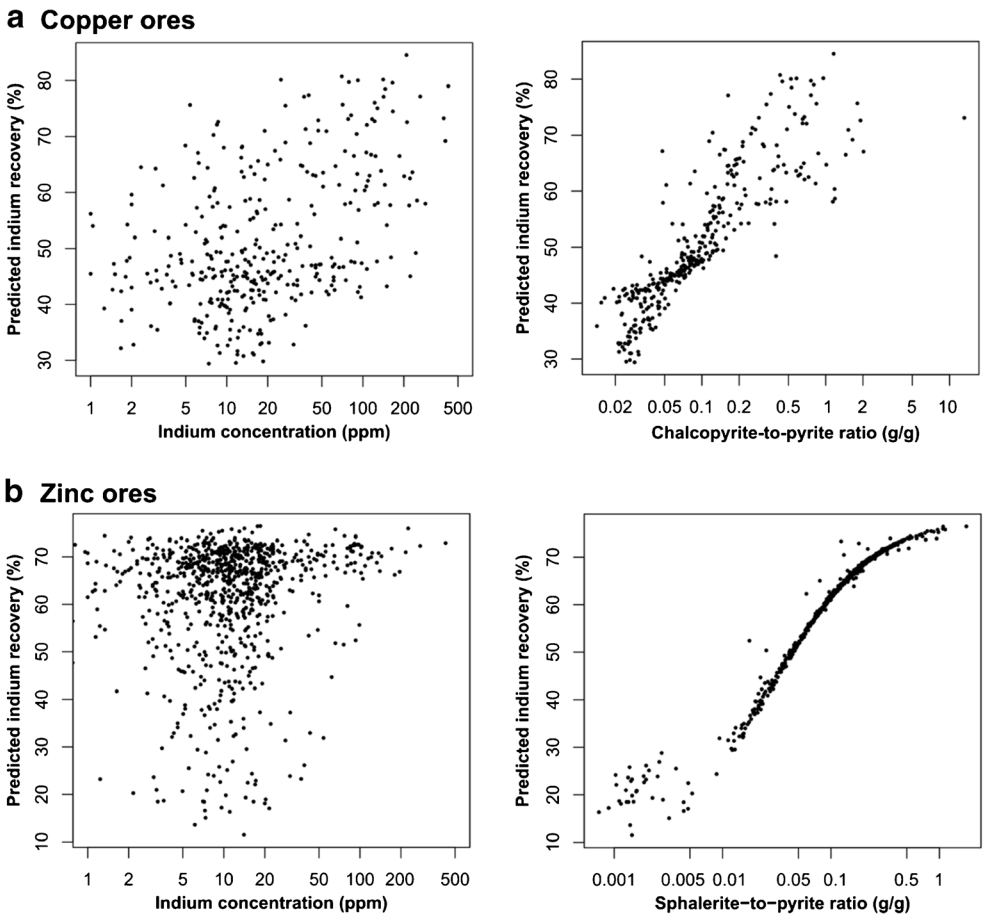

Fig. 14 Predicted indium recovery for drill core samples as a function of indium concentration in ore (left) and ore mineralogy (right) for **a** copper and **b** zinc ores

strong positive correlation of predicted recovery with the sphalerite-to-pyrite and chalcopyrite-to-pyrite ratios.

The weak correlation between indium grade and predicted recovery is likely a function of an underlying dependence between mineralogy and indium grade: ores with high copper and zinc grades also tend to have higher indium concentrations (cf. Carvalho et al. 2018). More of the indium hosted in these ores is recoverable, due to higher ratios of chalcopyrite and sphalerite to pyrite. Furthermore, the general effect that higher-grade ores tend to show higher recoveries due to more favorable mineral intergrowths (Wills and Finch 2015) should tend to further enhance this behavior. Therefore, indium recoveries for ores with high indium grades are expected to be higher.

Indium distribution within the deposit and control of indium grades in concentrates

A key factor for the commercialization of the indium content is the grade reached in concentrate streams. This is, because only concentrate grades above a certain minimum threshold are recoverable, and thus payable, by smelters (cf. Frenzel et al. 2017). It is therefore beneficial for the mine to be able to control concentrate grades by selectively mining or processing specific parts of the deposit sufficiently enriched in indium. However, whether this is practical or not depends on the specific distribution of indium across the deposit.

Figure 15 shows histograms of indium concentrations in the same set of 1231 drill core samples used for recovery predictions in the previous subsection (Fig. 14). Alongside the histograms, Fig. 15 shows cumulative distribution curves for indium. For the zinc ores, half of all indium is contained in samples with grades > 25 ppm indium (13% of all samples), while for the copper ores, half of all indium is hosted in samples with > 100 ppm indium (12% of all samples). Because these indium-rich ores occur in relatively large, coherent zones within the deposit (Carvalho et al. 2018) separate mining and processing could be feasible, e.g., by selective stockpiling.

Indium-rich ores are expected to produce concentrates with higher indium grades. This relationship is illustrated in Table 3 where we give estimates of the indium concentrations in hypothetical copper and zinc concentrates produced from ores with indium concentrations above certain cut-off grades. To compile these estimates, we simulated a mechanical mixture of equal parts of the samples above cut-off grade (including predicted deportments for each sample) to provide estimates of the mineralogical composition of, and indium deportment in, the resultant feed materials.

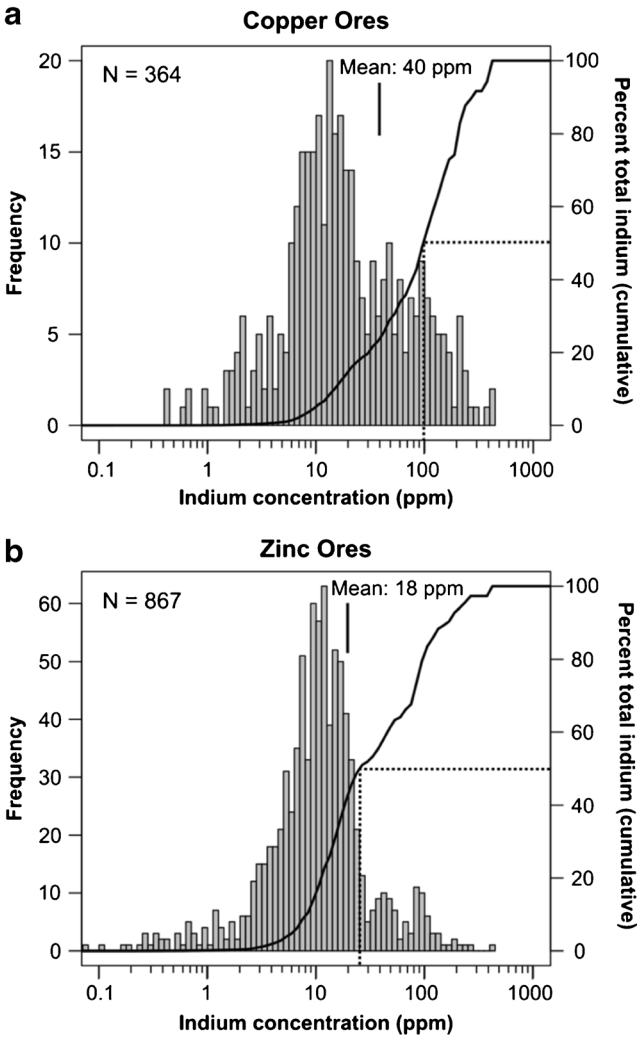

Fig. 15 Histograms of indium concentrations in drill-core samples of **a** copper and **b** zinc ores. The solid line shows the cumulative distribution of indium content, with the broken lines marking the concentration in each ore type for which half of all indium is contained in ores with a concentration above that value. The mean values shown by vertical arrows are the arithmetic means of the distributions. Samples with concentrations below detection limit were imputed randomly using a normal distribution with mean 10 ppm, and standard deviation 7 ppm, to reflect the uncertainties in their exact values

It is clear from the values in Table 3 that the selective processing of indium-rich ores could be used to produce concentrates with significantly higher indium concentrations than are currently produced. These would still contain a substantial proportion of the overall indium content of the deposit. While the exact cut-off grades for payable indium used by the smelters processing Neves-Corvo concentrates are confidential, it is nevertheless obvious that all predicted zinc concentrates, and most copper concentrates, easily

Table 3 Predicted concentrate grades and indium recoveries for the separate processing of indium-rich ores

Ore type	Cut-off (ppm In)	Pct. total indium (%)	Mean indium concentration (ppm)	Predicted Cu concentrate grade (ppm In)	Predicted Zn concentrate grade (ppm In)	Predicted indium recovery (%)[a]
Zn ores	0	100	18[b]	79	110	60
	25	50	73	300	360	63
	50	38	106	380	470	64
	75	32	121	420	530	65
	100	18	161	550	720	65
Cu ores	0	100	40	170	300	61
	25	82	96	300	570	64
	50	70	128	340	670	65
	75	60	152	340	720	67
	100	49	178	340	740	68

[a] Predicted recoveries are for the overall process (i.e., including Zn, Cu, and, where applicable, Pb concentrates)

[b] This value for the mean indium concentration of the Zn ores is more representative of the deposit than the mean value of 46 ppm attained by feed materials in June to August 2013 (cf. Carvalho et al. 2018)

achieve the minimum grades required for commercial indium extraction (~ 100 ppm In, cf. Frenzel et al. 2017). However, to be payable by smelters, higher grades are probably required. These should also be achievable.

As a final note, however, we emphasize that because indium recoveries depend on the behavior of the major ore and gangue minerals (mostly sphalerite, chalcopyrite, and pyrite), indium recoveries will change if the recoveries of these minerals change. Real recoveries may therefore differ from those predicted in Table 3 depending on actual plant performance. A full geometallurgical model would need to include models for the prediction of the recoveries of the major minerals based on the characteristics of individual mining blocks in addition to our deportment model.

Summary and conclusions

Based on a combination of bulk-ore geochemistry and mineralogical and microanalytical data, this study is the first to develop a quantitative model of indium deportment in the ores of a major sulfide base-metal deposit, demonstrating how regularities in indium partitioning between different sulfide minerals can be used to predict its mineralogical deportment in individual drill-core samples (1-m intervals) and mined blocks. Due to the well-constrained bulk mineralogy of the investigated ores, whole-ore assays of As, Cu, Fe, Pb, S, Sb, Sn, Zn, and In are sufficient for predictions with reasonable accuracy. The movement of indium through the ore processing plants is fully explained by its mineralogical deportment. Therefore, the predictive deportment models developed in this study are useful for mine planning and process design.

While sphalerite and chalcopyrite together are the most important indium carriers at Neves-Corvo, indium losses to tailings are mostly controlled by indium hosted in, or otherwise associated with, pyrite. In the ores, this fraction is between < 10 and 50%. As a result, indium recoveries are significantly below the recoveries of copper and zinc (overall recoveries of 81–86% for Cu, and 70–75% for Zn, but only 52–64% for In).

Our approach is of general applicability to other trace elements and ore types not just indium or specific by-products in base-metal sulfide ores. Once deportments can be reliably predicted, the use of these predicted deportments in mine planning and process control is quite straightforward. We note, however, that our model merely represents a starting point for further work. Its integration into a full-scale geometallurgical model would require the continuous updating of relevant parameters with actual operational results, as well as further models predicting plant performance for the major minerals.

Acknowledgments We would like to thank Bernd Lehmann, Julie Hunt, and two anonymous reviewers for their constructive comments that helped to significantly improve this manuscript. We are also greatly

indebted to our home institutions for their continued support without which the completion of this work would not have been possible. SOMINCOR is thanked for granting us access to Neves-Corvo mine, including drill core inventories and mine databases, as well as collecting the processing samples. The preparation team of HIF is thanked for their help with sample preparation. We also gratefully acknowledge the help of Michael Gäbelein who conducted some of the MLA and EPMA measurements. This is a contribution to the ZHINC project (PTDC/CTE-GIX/114208/2009) funded by the Portuguese agency FCT (Fundação para a Ciência e Tecnologia).

References

Bachmann K, Frenzel M, Krause J, Gutzmer J (2017) Advanced identification and quantification of in-bearing minerals by scanning electron microscope-based image analysis. Microsc Microanal 23:527–537

Barnes S-J, Prichard HM, Cox RA, Fisher PC, Godel B (2008) The location of the chalcophile and siderophile elements in platinum-group element ore deposits (a textural, microbeam and whole rock geochemical study): implications for the formation of deposits. Chem Geol 248:295–317

Benzaazoua M, Marion P, Liouville-Bourgeois L, Joussement R, Houot R, Franco A, Pinto A (2002) Mineralogical distribution of some minor and trace elements during laboratory flotation processing of Neves-Corvo ore (Portugal). Int J Miner Process 66:163–181

Benzaazoua M, Marion P, Pinto A, Migeon H, Wagner FE (2003) Tin and indium mineralogy within selected samples from the Neves Corvo deposit (Portugal): a multidisciplinary study. Miner Eng 16:1291–1302

Boisvert JB, Rossi ME, Ehrig K, Deutsch CV (2013) Geometallurgical modeling at Olympic Dam Mine, South Australia. Math Geosci 45: 901–925

Boorman RS, Abbott D (1967) Indium in co-existing minerals from the Mount Pleasant tin deposit. Can Mineral 9:166–179

Burnham CW (1959) Metallogenic provinces of the southwestern United States and northern Mexico. Bull New Mex Bur Min Mineral Resour 65

Cabri LJ, Campbell JL, La Flamme JHG, Leigh RG, Maxwell JA (1985) Proton-microprobe analysis of trace elements in sulfides from massive-sulfide deposits. Can Mineral 23:133–148

Cabri LJ, Wilson JMD, Distler VV, Kingston D, Nejedlý Z, Sluzheniken SF (2002) Mineralogical distribution of trace platinum-group elements in the disseminated sulphide ores of Noril'sk 1 layered intrusion. Appl Earth Sci 111:15–22

Carvalho JRS, Fernandes AS, Moreira BB, Pinto ÁMM, Relvas JMRS, Pacheco NP, Pinto F, Fonseca R (2013) Hydrothermal alteration and ore mineralogy at the Lombador massive sulphide orebody, Neves Corvo, Portugal: an on-going study. In: Jonsson E et al. (eds) Mineral deposit research for a high-tech world, In: Proceedings of the 12th SGA biennial meeting, Uppsala, Sweden, pp 514–517

Carvalho JRS, Relvas JMRS, Pinto ÁMM, Pacheco N, Fonseca R, Santos S, Caetano CP, Reis T, Gonçalves M (2015) On the indium and selenium distribution and mineral allocation at the Neves Corvo deposit, Portugal. In: André-Meyer S-A et al. (eds) Mineral resources in a sustainable world. Proceedings of the 13th SGA biennial meeting, Nancy, France, pp 695–698

Carvalho JRS, Relvas JMRS, Pinto AMM, Frenzel M, Krause J, Gutzmer J, Pacheco N, Fonseca R, Santos S, Caetano CP, Reis T, Goncalves M (2018) Indium and selenium distribution in the Neves-Corvo deposit, Iberian Pyrite Belt, Portugal. Mineral Mag 82:S5–S41

Carvalho P, Ferreira A (1994) Geologia de Neves-Corvo: estado actual do conhecimento. 4th Simpósio de Sulfuretos Polimetálicos da Faixa Piritosa Ibérica, Évora, Portgual

Chen TT, Petruk W (1980) Mineralogy and characteristics that affect recoveries of metals and trace elements from the ore at heath steele mines. New Brunswick CIM Bull 73:167–179

Chryssoulis SL, Cabri LJ (1990) Significance of gold mineralogical balances in mineral processing. T I Min Metall C 99:1–10

Cook NJ, Ciobanu CL, Pring A, Skinner W, Shimizu M, Danyushevsky L, Saini-Eidukat B, Melcher F (2009) Trace and minor elements in sphalerite: a LA-ICPMS study. Geochim Cosmochim Ac 73:4761–4791

Cook NJ, Ciobanu CL, Danyushevsky L, Gilbert S (2011a) Minor and trace elements in bornite and associated Cu-(Fe)-sulfides: a LA-ICP-MS study. Geochim Cosmochim Ac 75:6473–6496

Cook NJ, Sundblad K, Valkama M, Nygard R, Ciobanu CL, Danyushevsky L (2011b) Indium mineralisation in A-type granites in southeastern Finland: insights into mineralogy and partitioning between coexisting minerals. Chem Geol 284:62–73

EU Commission (2017) Study on the review of the list of critical raw materials. European Commission, Brussels

Fandrich R, Gu Y, Burrows D, Moeller K (2007) Modern SEM-based mineral liberation analysis. Int J Miner Process 84:310–320

Frenzel M, Mikolajczak C, Reuter MA, Gutzmer J (2017) Quantifying the relative availability of high-tech by-product metals—the cases of gallium, germanium and indium. Resour Policy 52:327–335

Gaspar OC (2002) Mineralogy and sulfide mineral chemistry of the Neves-Corvo ores, Portugal: insight into their genesis. Can Mineral 40:611–636

Gaspar O, Pinto A (1991) The ore textures of the Neves-Corvo volcanogenic massive sulphides and their implications for ore beneficiation. Mineral Mag 55:417–422

George LL, Cook NJ, Ciobanu CL (2016) Partitioning of trace elements in co-crytallised sphalerite-galena-chalcopyrite hydrothermal ores. Ore Geol Rev 77:97–116

Goodall WR (2008) Characterisation of mineralogy and gold deportment for complex tailings deposits using QEMSCAN. Miner Eng 21:518–523

Graedel TE, Harper EM, Nassar NT, Nuss P, Reck BK (2015) Criticality of metals and metalloids. P Natl Acad Sci USA 112: 4257–4262

Gregory MJ, Lang JR, Gilbert S, Hoal KO (2013) Geometallurgy of the pebble porphyry copper-gold-molybdenum deposit, Alaska: implications for gold distribution and paragenesis. Econ Geol 108:463–482

Gurmendi AC (2013) The minerals industry of Portugal. In: USGS minerals yearbook 2011. U.S. Geological Survey, Reston 36.1–36.6

Heinig T, Bachmann K, Tolosana-Delgado R, van den Boogaart G, Gutzmer J (2015) Monitoring gravitational and particle shape settling effects on MLA sampling preparation. In: Proceedings of the 18th annual IAMG conference, Freiberg. IAMG, Houston, pp 200–206

Huston DL, Sie SH, Suter GF, Cooke DR, Both RA (1995) Trace elements in sulfide minerals from eastern Australian volcanic-hosted massive sulfide deposits. Part I. Proton microprobe analyses of pyrite, chalcopyrite, and sphalerite/Part II. Selenium levels in pyrite: comparison with δ34S values and implications for the source of sulfur in volcanogenic hydrothermal systems. Econ Geol 90:1167–1196

James F (1980) Monte Carlo theory and practice. Rep Prog Phys 43: 1145–1189

Kern M, Möckel R, Krause J, Teichmann J, Gutzmer J (2018) Calculating the deportment of a fine-grained and compositionally complex Sn skarn with a modified approach for automated mineralogy. Miner Eng 116:213–225

Lockington JA, Cook NJ, Ciobanu CL (2014) Trace and minor elements in sphalerite from metamorphosed sulphide deposits. Miner Petrol 108:873–890

Lundin (2017) Annual information form for the year ended December 31, 2016. Lundin Mining, Toronto

Mariano RA, Evans CL (2015) Error analysis in ore particle composition distribution measurements. Miner Eng 82:36–44

Minz FE, Bolin N-J, Lamberg P, Bachmann K, Gutzmer J, Wanhainen C (2015) Distribution of Sb minerals in the Cu and Zn flotation of Rockliden massive sulphide ore in North-Central Sweden. Miner Eng 82:125–135

Mosier DL, Berger VI, Singer DA (2009) Volcanogenic massive sulfide deposits of the world—database and grade and tonnage models. USGS Open File Report 2009-1034

Munhá J (1990) Metamorphic evolution of the south Portuguese/Pulo do Lobo Zone. In: Dallmeyer RD, Martinez Garcia E (eds) Pre-Mesozoic geology of Iberia. Springer-Verlag, Berlin, pp 363–368

Murakami H, Ishihara S (2013) Trace elements of indium-bearing sphalerite from tin polymetallic deposits in Bolivia, China and Japan: a femto-second LA-ICP-MS study. Ore Geol Rev 53:223–243

Nassar NT, Graedel TE, Harper EM (2015) By-product metals are technologically essential but have problematic supply. Sci Adv 1: e1400180

Newall P, Hill A, Ellis R, King P, Holley S et al. (2017) NI 43-101 technical report for the Neves-Corvo mine, Portugal. Wardell Armstrong International Ltd, Stoke-on-Trent

NSTC (2016) Assessment of critical minerals: screening methodology and initial application. Subcommittee on critical and strategic mineral supply chains of the committee on environment. Natural Resources and Sustainability of the National Science and Technology Council, Washington, DC

Ohta E (1989) Occurrence and chemistry of indium-containing minerals from the Toyoha mine, Hokkaido, Japan. Mining Geol 39: 355–372

Oliveira JT, Pereira Z, Carvalho P, Pacheco N, Korn D (2004) Stratigraphy of the tectonically imbricated lithological succession of the Neves Corvo mine are, Iberian Pyrite Belt, Portugal. Mineral Deposita 39:422–436

Osbahr I, Klemd R, Oberthür T, Brätz H, Schouwstra R (2013) Platinum-group element distribution in base-metal sulfides of the Merensky Reef from the eastern and western Bushveld Complex, South Africa. Mineral Deposita 48:211–232

Osbahr I, Oberthür T, Klemd R, Josties A (2014) Platinum-group element distribution in base-metal sulfides of the UG2 chromitite, Bushveld Complex, South Africa—a reconnaissance study. Mineral Deposita 49:655–665

Owen ML, Chilcott DL (2007) Technical report on the Neves Corvo Mine, Portugal. Wardell Armstrong International Ltd., Truro

Owen ML, Meyer L (2013) NI 43-101 technical report for Neves-Corvo Mine and Semblana Deposit, Portugal. Wardell Armstrong International Ltd., Truro

Pacheco N, Carvalho P, Ferreira A (1998) Geologia da Mina de Neves Corvo e do vulcanismo do anticlinório de Panóias—Castro Verde. In: Oliveira JT, Dias R (eds) Guia das Excursões: V Congresso Nacional de Geologia

Petruk W, Schnarr JR (1981) An evaluation of the recovery of free and unliberated mineral grains, metals and trace elements in the concentrator of Brunswick Mining and Smelting Corp. Ltd CIM Bull 74:132–159

Relvas JMRS, Barriga FJAS, Ferreira A, Noiva PC, Pacheco N, Barriga G (2006a) Hydrothermal alteration and mineralization in the Neves-Corvo volcanic-hosted massive sulfide deposit, Portugal. I. Geology, mineralogy, and geochemistry. Econ Geol 101:753–790

Relvas JMRS, Barriga FJAS, Longstaffe FJ (2006b) Hydrothermal alteration and mineralization in the Neves-Corvo volcanic-hosted massive sulfide deposit, Portugal. II. Oxygen, hydrogen, and carbon isotopes. Econ Geol 101:791–804

Rosa CJP, McPhie J, Relvas JMRS, Pereira Z, Oliveira T, Pacheco N (2008) Facies analyses and volcanic setting of the giant Neves Corvo massive sulfide deposit, Iberian Pyrite Belt, Portugal. Mineral Deposita 43:449–466

Schwarz-Schampera U, Herzig P (2002) Indium—geology, mineralogy, economics. Springer-Verlag, Berlin

Seifert T, Sandmann S (2006) Mineralogy and geochemistry of indium-bearing polymetallic vein-type deposits: implications for host minerals form the Freiberg district, eastern Erzgebirge, Germany. Ore Geol Rev 28:1–31

Serranti S, Ferrini V, Masi U, Cabri LJ (2002) Trace-element distribution in cassiterite and sulfides from rubané and massive ores of the Corvo deposit, Portugal. Can Mineral 40:815–835

Sinclair WD, Kooiman GJA, Martin DA, Kjarsgaard IM (2006) Geology, geochemistry and mineralogy of indium resources at Mount Pleasant, New Brunswick, Canada. Ore Geol Rev 28: 123–145

Tolcin AC (2017) Indium. In: USGS mineral commodity summaries. U.S. Geological Survey, Reston, pp 80–81

Tornos F (2006) Environment of formation and styles of volcanogenic massive sulfides: the Iberian Pyrite Belt. Ore Geol Rev 28:259–307

Van den Boogaart KG, Tolosana-Delgado R (2013) Analyzing compositional data with R. Springer-Verlag, Berlin

Wellmer F-W, Hannak W, Krauss U, Thormann A (1990) Deposits of rare metals. In: Kürsten M (ed) Raw materials for new technologies. Proceedings of the fifth international symposium, held in Hannover, Fed. Rep. of Germany, at the Federal

Institute for Geosciences and Natural Resources, October 19–21, 1988, Schweizerbart, Stuttgart, pp 71–122

Werner TT, Mudd GM, Jowitt SM (2017) The world's by-product and critical metal resources part III: a global assessment of indium. Ore Geol Rev 86:939–956

Wills BA, Finch JA (2015) Wills' mineral processing technology: an introduction to the practical aspects of ore treatment and mineral recovery. Elsevier, Amsterdam

Ye L, Cook NJ, Ciobanu CL, Yuping L, Qian Z, Tiegeng L, Wei G, Yulon Y, Danyushevsky L (2011) Trace and minor elements in sphalerite from base metal deposits in South China: a LA-ICP-MS study. Ore Geol Rev 39:188–217

Yi W, Halliday A, Lee D-C, Christensen JN (1995) Indium and tin in basalts, sulfides, and the mantle. Geochim Cosmochim Ac 59: 5081–5090